Cell Reports
Medicine

Article

In vivo vulnerabilities to GPX4 and HDAC inhibitors in drug-persistent versus drug-resistant BRAF^{V600E} lung adenocarcinoma

Graphical abstract

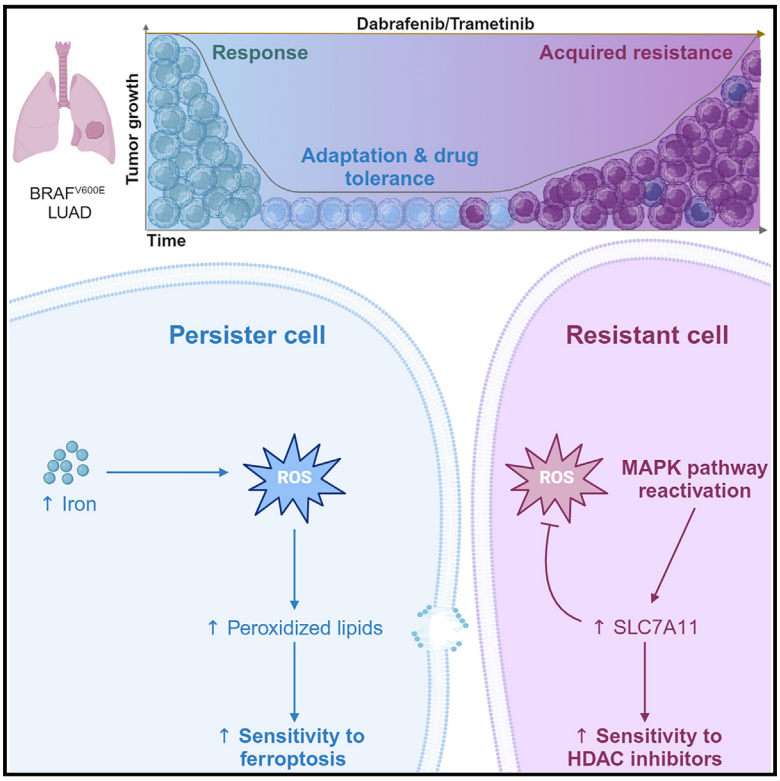

Highlights

- Unbiased genetic screen identifies ferroptosis as DTP vulnerability in *BRAF*^{V600E} LUAD
- GPX4 inhibitors extend survival when applied at early disease relapse
- Relapsed tumors display biomarkers indicative of sensitivity to ferroptosis triggers
- Acquired mutations restoring MAPK signaling sensitize tumors to HDAC inhibition

Authors

Marie-Julie Nokin, Elodie Darbo, Elodie Richard, ..., Chiara Ambrogio, David Santamaría, Bolero Consortium

Correspondence

mjnokin@uliege.be (M.-J.N.), chiara.ambrogio@unito.it (C.A.), d.santamaria@usal.es (D.S.)

In brief

Nokin et al. identify two redox-related cellular states that involve an adaptive drug-tolerant stage followed by a genetic-defined resistance phase in *BRAF*^{V600E}-driven lung cancer. Timely treatments with small molecules (GPX4 and HDAC inhibitors) that further enhance the resulting oxidative stress delay disease progression *in vivo*.

Nokin et al., 2024, Cell Reports Medicine *5*, 101663
August 20, 2024
https://doi.org/10.1016/j.xcrm.2024.101663

CellPress

Cell Reports Medicine

CellPress
OPEN ACCESS

Article

In vivo vulnerabilities to GPX4 and HDAC inhibitors in drug-persistent versus drug-resistant BRAF^{V600E} lung adenocarcinoma

Marie-Julie Nokin,[1,2,*] Elodie Darbo,[3] Elodie Richard,[3] Sonia San José,[1,4] Sergio de Hita,[1,3,4] Valérie Prouzet-Mauleon,[3,5] Béatrice Turcq,[3,5] Laura Gerardelli,[2] Rebekah Crake,[2] Valérie Velasco,[6] Benjamin Koopmansch,[7] Frederic Lambert,[7] Jenny Y. Xue,[8] Ben Sang,[8] Julie Horne,[9] Eric Ziemons,[9] Alberto Villanueva,[10] Arnaud Blomme,[11] Michael Herfs,[12] Didier Cataldo,[2] Olivier Calvayrac,[13] Paolo Porporato,[14] Ernest Nadal,[15] Piro Lito,[8] Pasi A. Jänne,[16] Biagio Ricciuti,[16] Mark M. Awad,[16] Chiara Ambrogio,[14,*] David Santamaría,[1,4,17,*] and Bolero Consortium

[1]University of Bordeaux, INSERM U1218, ACTION Laboratory, IECB, 33600 Pessac, France
[2]Laboratory of Biology of Tumor and Development (LBTD), GIGA-Cancer, University of Liege, 4000 Liege, Belgium
[3]Bordeaux Institute of Oncology (BRIC), INSERM U1312, University of Bordeaux, 33000 Bordeaux, France
[4]Centro de Investigación del Cáncer, CSIC-Universidad de Salamanca, 37007 Salamanca, Spain
[5]CRISP'edit, TBMCore, University of Bordeaux, CNRS UAR 3427, INSERM US05, 33000 Bordeaux, France
[6]Department of Biopathology, Institut Bergonié, 33076 Bordeaux, France
[7]Department of Human Genetics, University Hospital Center of Liege, 4000 Liege, Belgium
[8]Department of Medicine, Memorial Sloan Kettering Cancer Center, New York, NY 10065, USA
[9]Laboratory of Pharmaceutical Analytical Chemistry, CIRM, University of Liege, 4000 Liege, Belgium
[10]Chemoresistance and Predictive Factors Group, Program Against Cancer Therapeutic Resistance (ProCURE), Catalan Institute of Oncology (ICO); Oncobell Program, Bellvitge Biomedical Research Institute (IDIBELL), L'Hospitalet del Llobregat, 08908 Barcelona, Spain
[11]Laboratory of Cancer Signaling, GIGA-Stem Cells, University of Liege, 4000 Liege, Belgium
[12]Laboratory of Experimental Pathology, GIGA-Cancer, University of Liege, 4000 Liege, Belgium
[13]Cancer Research Centre of Toulouse, INSERM UMR1037, CNRS UMR5071, 31100 Toulouse, France
[14]Department of Molecular Biotechnology and Health Sciences, Molecular Biotechnology Center, University of Torino, 10126 Torino, Italy
[15]Molecular Mechanisms of Cancer Program, Department of Medical Oncology, Catalan Institute of Oncology (ICO), Preclinical and Experimental Research in Thoracic Tumors (PReTT) Group, Oncobell Program, IDIBELL, L'Hospitalet del Llobregat, 08908 Barcelona, Spain
[16]Department of Medical Oncology, Dana–Farber Cancer Institute, Boston, MA 02215, USA
[17]Lead contact
*Correspondence: mjnokin@uliege.be (M.-J.N.), chiara.ambrogio@unito.it (C.A.), d.santamaria@usal.es (D.S.)
https://doi.org/10.1016/j.xcrm.2024.101663

SUMMARY

The current targeted therapy for *BRAF*^{V600E}-mutant lung cancer consists of a dual blockade of RAF/MEK kinases often combining dabrafenib/trametinib (D/T). This regimen extends survival when compared to single-agent treatments, but disease progression is unavoidable. By using whole-genome CRISPR screening and RNA sequencing, we characterize the vulnerabilities of both persister and D/T-resistant cellular models. Oxidative stress together with concomitant induction of antioxidant responses is boosted by D/T treatment. However, the nature of the oxidative damage, the choice of redox detoxification systems, and the resulting therapeutic vulnerabilities display stage-specific differences. Persister cells suffer from lipid peroxidation and are sensitive to ferroptosis upon GPX4 inhibition *in vivo*. Biomarkers of lipid peroxidation are detected in clinical samples following D/T treatment. Acquired alterations leading to mitogen-activated protein kinase (MAPK) reactivation enhance cystine transport to boost GPX4-independent antioxidant responses. Similarly to BRAF^{V600E}-mutant melanoma, histone deacetylase (HDAC) inhibitors decrease D/T-resistant cell viability and extend therapeutic response *in vivo*.

INTRODUCTION

The RAF family of serine/threonine kinases is comprised by three isoforms (A-, B-, and CRAF). They are known for mediating RAS activation to the downstream kinases MEK and ERK with few additional substrates. In spite of sharing such stringent substrate specificity, a similar activation mechanism, and the presence of three highly conserved regions, their implication in human cancer is strikingly different.[1] While both mutations and oncogenic fusions implicating *A*- and *CRAF* have been identified in human tumors, they appear at a much lower frequency than those involving *BRAF*. Over 200 *BRAF* cancer-related mutations have been identified and are subdivided in three classes with different clinical properties.[2,3] The most common substitution

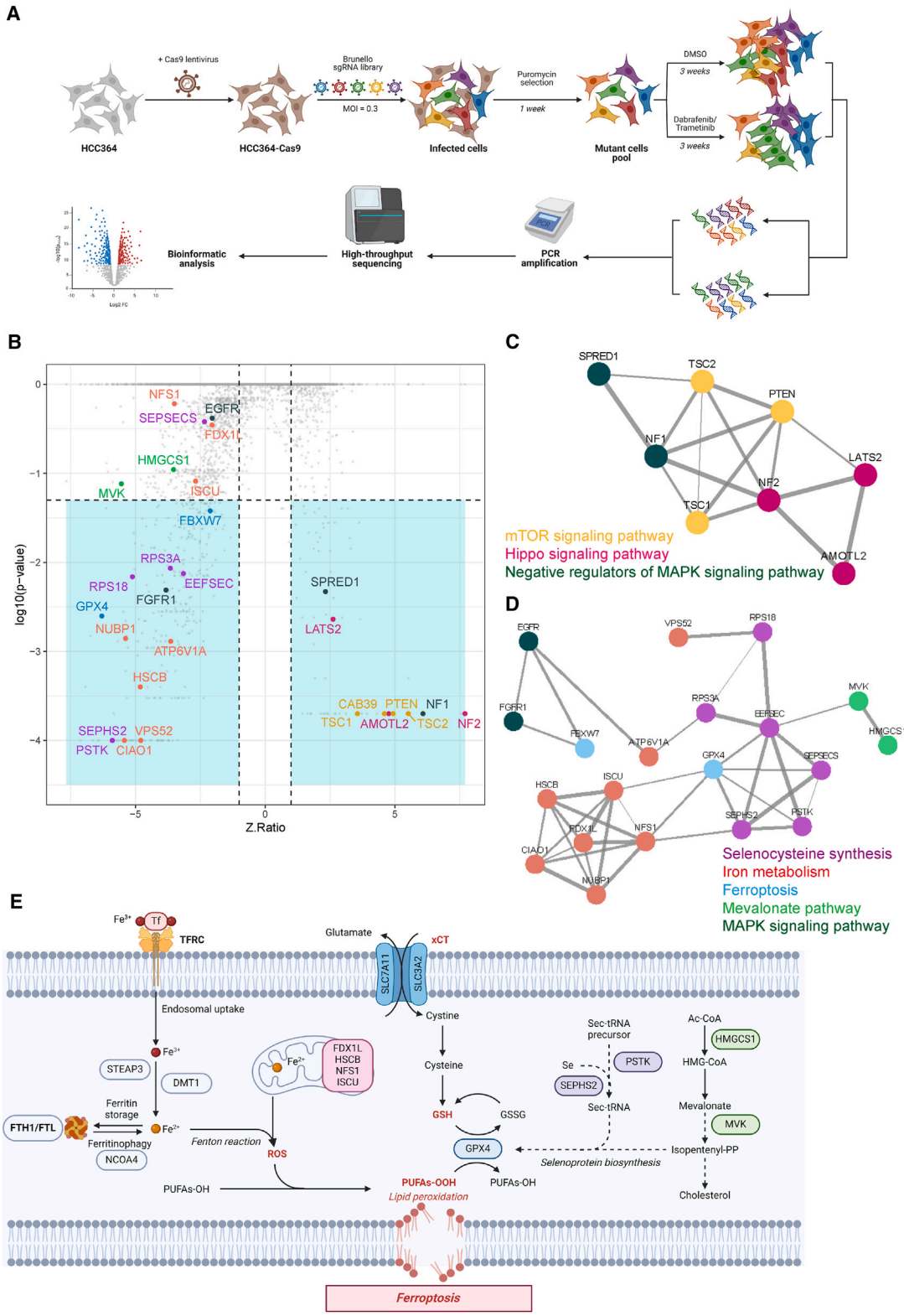

Figure 1. Genome-wide CRISPR-Cas9 screening identifies determinants of dabrafenib/trametinib sensitivity in *BRAF*-mutant LUAD cells

(A) Schematic diagram illustrates the genome-wide CRISPR-Cas9 knockout library screening. Human Brunello sgRNA library was packed into lentiviral particles and transduced into Cas9-overexpressing HCC364 cells (HCC364-Cas9). The sgRNA-transduced cells were selected by puromycin and cultured in vehicle and

(legend continued on next page)

(V600E) belongs to the class 1 and mimics phosphorylation of the activation loop resulting in constitutive signaling as an active monomer in an RAS-independent manner. In lung adenocarcinoma (LUAD), *BRAF* mutations are detected in approximately 5% of cases with a balanced representation of V600E and non-V600E events. Yet, only V600E patients are treated with targeted agents.[4] The standard of care consists of a dual blockade of RAF/MEK kinases often combining dabrafenib with trametinib (hereafter referred as D/T) resulting in higher response rate and extended progression-free survival when compared to single-agent treatments.[5] However, as with other targeted treatments, tumor progression will eventually occur. A fraction of resistant tumors display mutations in other members of the RAS-ERK pathway resulting in reactivated signaling.[6,7] These alterations co-exist with the original $BRAF^{V600E}$ driver, and it is unknown whether, as observed in patients with melanoma, the oncogenic combination could drive relapse at the expense of acquiring novel targetable vulnerabilities.[8] Furthermore, there is limited information of how $BRAF^{V600E}$-driven LUAD tumors adapt to D/T treatment and whether this is accompanied by actionable vulnerabilities.

Here, we combined naive $BRAF^{V600E}$ lung cancer cell lines as well as patient-derived xenograft (PDX) cell cultures with acquired D/T resistance *in vivo*, CRISPR-Cas9 screening, and pharmacological treatments to identify mechanisms of resistance and associated vulnerabilities that could potentially be implemented to fight disease relapse in the clinic.

RESULTS

Genome-wide screen to identify mediators and molecular vulnerabilities upon D/T treatment

We used the LUAD $BRAF^{V600E}$-mutant HCC364 human cell line to generate a Cas9 derivative by lentiviral delivery of the enzyme. The growth properties and the response to D/T of the Cas9-expressing cells were indistinguishable from the parental cell line (data not shown). To perform the screen, we selected the lentiviral CRISPRko sgRNA Brunello library.[9] It was transduced into cells at a multiplicity of infection of 0.3 and 1,000× coverage and selected with puromycin during 1 week before being divided into control and D/T-treated groups. D/T treatment was performed using the IC50 values obtained for each individual compound (Figures S1A and S1B). This D/T combination induced an apoptotic response together with a fraction of surviving cells (Figure S1C) that were maintained during 3 weeks to enable positive and negative selection of single-guide RNAs (sgRNAs) compared to control conditions. At this point, the genomic DNA was harvested, and the sgRNA cassette was amplified and quantitated by Illumina sequencing (Figure 1A).

Bioinformatic comparisons using CRISPRAnalyzeR[10] were performed to identify sgRNAs that appeared with differential representative scores (Figure 1B). The biological significance of the screening was confirmed by the identification of FBXW7, whose inactivation has been reported to elicit a multidrug resistance phenotype.[11] The screen also identified several enriched and depleted sgRNAs targeting genes previously reported to mediate D/T resistance or to induce increased sensitivity, respectively. Among the most relevant enriched sgRNAs, we found those targeting negative regulators of the mitogen-activated protein kinase (MAPK) and PI3K pathways as well as inhibitors of the YAP transcriptional program (Figure 1B). In good agreement, sgRNAs directed against genes implicated in the activation of these processes or pathway effectors required for effective signaling appeared as drop-out hits. In sum, these results validate our genetic screen by confirming previous findings indicating that RTK/RAS-dependent hyperactivation of MAPK and PI3K signaling or elevated Hippo pathway activity results in D/T resistance[6,12–16] (Figure 1C).

Lipid peroxidation as an early phenotype and potential vulnerability following D/T treatment

To identify therapeutic vulnerabilities associated with D/T adaptation, we further investigated the list of depleted sgRNAs following treatment. One of the most prominent candidates was GPX4 (ninth out of 736 significantly depleted sgRNAs) with a Z-ratio of −6.30 (Figure 1B). Interestingly, GPX4 has been reported to play an essential pro-survival function to sustain an early therapy-resistant cell state in a variety of tumor types and drug treatments.[17,18] GPX4 is a selenocysteine-containing enzyme with lipid hydroperoxidase function essential to protect cells from ferroptosis, an iron-mediated oxidative form of cell death.[19] In good agreement, we identified a collection of depleted guides converging on three biological processes functionally related to GPX4 and ferroptosis: selenocysteine synthesis, mevalonate pathway (e.g., PSTK, SEPSH2, MVK, and HMGCS1), and iron metabolism (e.g., FDX1L, HCSB, NFS1, and ISCU) (Figures 1D and 1E).

Drug treatments often induce a non-mutational drug-tolerant persister (DTP) transient state characterized by low proliferation rates. Over time, a subset of DTPs gradually resumes proliferation in the presence of the drug, originating a second population of cells known as drug-tolerant expanded persisters (DTEPs).[20,21] Collectively, these populations provide a cellular reservoir from which acquired drug resistance mechanisms eventually unfold.[21,22] We generated putative DTPs and DTEPs by maintaining $BRAF^{V600E}$-mutant HCC364 cells on constant D/T treatment for 3 and 40 weeks, respectively. The cells at the 3-week time point—that coincided with the end of the CRISPR screen (Figure 1A)—were in a non or low-cycling stage.

dabrafenib/trametinib (D/T) (250/5 nM, refreshed every 3 days) for 3 weeks. Genomic DNA was extracted from the treated cells and the sgRNA fragment was amplified by PCR. Copy number of sgRNAs was determined by high-throughput sequencing analysis.

(B) Scatterplot depicting gene-level results for D/T negatively and positively selected hits in the CRISPR screen. A number of representative hits are shown in color and are detailed in C and D. $n = 1$ biological replicate.

(C and D) STRING protein network of the positively (C) and negatively (D) selected hits as defined in (B). Colored nodes highlight proteins enriched in certain signaling pathways. The edges represent protein-protein associations, and the line thickness indicates the strength of data support. $n = 1$ biological replicate.

(E) Scheme representing the major actors of ferroptosis, highlighting the central role of GPX4 in the detoxification of peroxidized lipids. See also Figure S1.

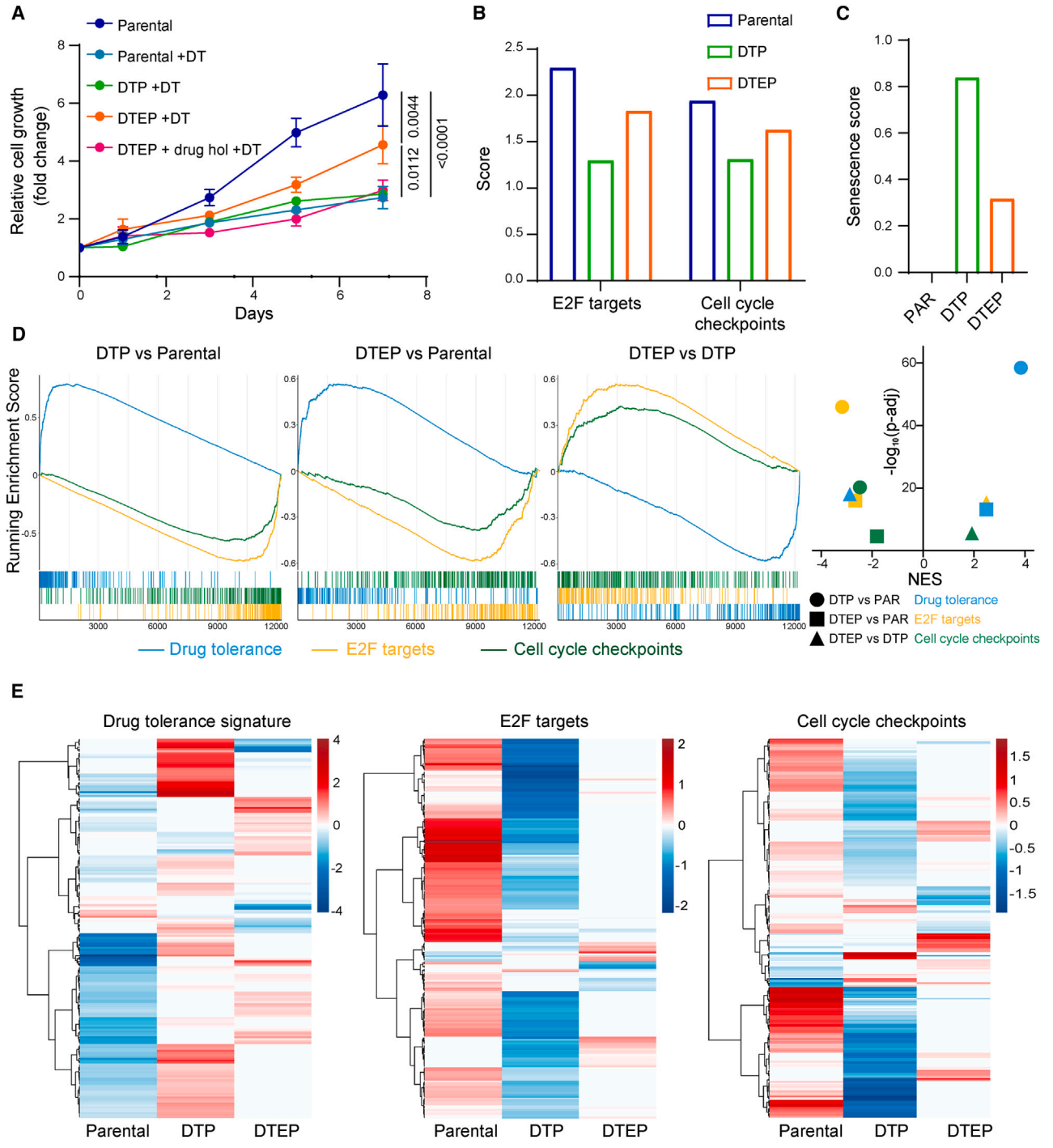

Figure 2. Transcriptomic analysis of drug-tolerant persister and drug-tolerant expanded persister HCC364 cells points to redox homeostasis as a potential vulnerability in these cell populations

(A) Drug-tolerant persisters (DTPs) and drug-tolerant expanded persisters (DTEPs) were generated by maintaining *BRAF*^{V600E}-mutant HCC364 cells on constant D/T (250/5 nM) treatment for 3 and 40 weeks, respectively. Growth curves of parental, DTP, and DTEP HCC364 cells in the presence of 250/5 nM D/T. DTEPs underwent a drug holiday for 3 weeks and were rechallenged with D/T to further confirm the non-genetic adaptation of these cells to the treatment (DTEP + drug hol + D/T). Data were analyzed using two-way ANOVA followed by Tukey's multiple comparisons post-test and are shown as the mean values ± SEM. *n* = 3 biological replicates.

(B) RNA sequencing analyses were performed on HCC364 parental, DTP, and DTEPs cells. E2F targets and cell cycle checkpoints ssGSEA scores in parental, DTP, and DTEP HCC364 cells. *n* = 1 biological replicate.

(legend continued on next page)

At the end of the screening process, the control population expanded 7,000-fold whereas the D/T-treated condition, potentially representing a DTP state, only increased by 1.5-fold. However, at 40 weeks on constant D/T treatment, the population displayed intermediate proliferation rates when compared to the parental controls and therefore potentially constituted a DTEP pool (Figure 2A). This different proliferation rate between DTP and DTEP cells was further confirmed by dissimilar enrichment scores of cell cycle-related terms (cell cycle checkpoints and e2F targets) using single-sample gene set enrichment analysis (ssGSEA) of RNA sequencing data (Figure 2B). In good agreement with previous reports,[17,20] our DTEPs reverted to a drug-sensitive state upon D/T removal (drug holiday for 3 weeks), indicating that cell proliferation in the presence of the drugs was sustained by non-mutational adaptation (Figure 2A). Furthermore, induction of cellular senescence is also one of the underlying mechanisms by which cancer therapies exert anti-tumor activity and could be an early trigger to dormancy.[23,24] We investigated the transcriptome of our DTP and DTEPs by applying SENCAN, a cancer senescence classifier.[25] In accordance with their respective proliferation rates, we observed a 3-fold increase in the senescence score in the DTP state, reinforcing the concept that persistent D/T treatment triggers a gradual and adaptive evolution with increased proliferative properties resulting in a DTEP population (Figure 2C). More reassuringly, we applied a recently developed transcriptional signature defining the DTP state composed of 212 genes commonly up-regulated in lung DTP models.[26] Following D/T treatment, our putative DTP and DTEP populations displayed an enrichment of the tolerance signature suggesting that their state is a *bona fide* persister phenotype (Figures 2D, 2E, and S1D).

In addition, gene set enrichment analysis (GSEA) pathway showed that modulation of seleno-aminoacid metabolism, cholesterol homeostasis, and oxidative stress were found in both DTPs and DTEPs (data not shown), thus pointing to redox homeostasis as a potential vulnerability in these cell populations. These data further support the potential dependency to GPX4-mediated detoxification of peroxidized lipids (highlighted by the CRISPR screen). Therefore, we next wanted to assess whether GPX4 function could be an essential feature during the entire period of drug-dependent cellular evolution and could consequently be a common vulnerability. Following D/T treatment, we observed a significant reduction in the redox-buffer potential measured by glutathione (GSH) cellular content with a concomitant increase in reactive oxygen species (ROS) in both populations (Figures 3A and 3B). Interestingly, this phenotype was accompanied by an elevation of both intracellular iron levels and peroxidized lipids that could explain their dependency on the GPX4 antioxidant function (Figures 3C and 3D). Importantly, D/T-treated cells displayed increased sensitivity to the GPX4 inhibitor RSL3 as well as to the ferroptosis activators erastin and FIN56 (Figures 3E, 3F, and 3G). In all cases, DTPs and DTEPs displayed enhanced sensitivity suggesting a higher GPX4 dependency. In agreement with the screen result, this sensitivity was further confirmed by CRISPR-mediated GPX4 depletion in the DTEP cells (Figure S2). Furthermore, the toxicity induced by RSL3 and erastin and the concomitant increase in lipid peroxidation were suppressed by co-treatment with the antioxidants N-acetylcysteine (NAC) and Trolox or with various ferroptosis inhibitors (liproxstatin, ferrostatin, and deferoxamine) reinforcing their increased sensitivity to ferroptosis (Figures 3H, 3I, and S3)

As mentioned earlier, the genetic screen and the RNA sequencing analysis identified biological processes that are mechanistically linked to GPX4 detoxification functions. These included components of the mevalonate pathway and selenoprotein biosynthesis as well as iron metabolism that could represent additional therapeutic vulnerabilities. The relevance of the selenoprotein biosynthetic pathway in this context was illustrated by the complete rescue of RSL3 sensitivity upon selenium supplementation (Figure 3J). Similarly, the mevalonate pathway provides essential precursors to selenoprotein biosynthesis, through the isopentenylation of selenocysteine-tRNA (Figure 1E).[27,28] In good agreement, targeting HMG-CoA reductase by several statins also affected DTEPs, although we failed to observe an additive effect when combined with GPX4 inhibition (Figure 4).

As a whole, these results demonstrate that following D/T treatment, *BRAF*^{V600E}-mutant LUAD persister cells display a disabled antioxidant program that renders them vulnerable to ferroptosis triggers.

Sensitivity of D/T persister cells to GPX4 inhibition *in vivo*

Evidence presented so far has identified the GPX4-antioxidant role as an essential pro-survival function during tumor adaptation upon D/T treatment and its inhibition as a potential therapy to target disease relapse. To further validate this hypothesis using a clinically relevant model, we utilized a *BRAF*^{V600E}-mutant cell line (clone 1D) generated from a PDX of lung cancer that progressed following treatment with an RAF inhibitor.[29] These cells were cultured with increasing concentrations of D/T starting from their respective IC50 values (Figures S1A and S1B) until they partially regained proliferative capacity and therefore reached a putative DTEP state (Figure 4A). Indeed, the sensitivity to D/T was partly restored following a drug holiday period suggesting that it was due to an adaptive mechanism. Remarkably, 1D-DTPs and 1D-DTEPs showed up to 30-fold increase in their sensitivity to RSL3 when compared to the parental controls (Figure 4B). 1D-DTEPs also presented an increased sensitivity to erastin (Figure S5A). In both contexts, cellular viability was restored by co-treatment with ferroptosis inhibitors, antioxidants, and selenium (Figures 4C and S5B). Similarly to HCC364 cells, 1D-DTEPs displayed increased ROS, peroxidized lipids, and intracellular iron levels (Figures S5C–S5E).

(C) Senescence score in parental (PAR), DTP, and DTEP HCC364 cells. $n = 1$ biological replicate.
(D) Running enrichment scores of GSEA (left panel) in DTP vs. PAR, DTEP vs. PAR, and DTEP vs. DTP using the drug tolerance signature and the E2F targets and cell cycle checkpoints gene sets. Normalized enrichment scores (NESs) against the log10 of adjusted p value are shown (right panel). $n = 1$ biological replicate.
(E) Heatmap of the significantly differentially expressed genes from the 3 gene sets (drug tolerance signature, E2F targets, and cell cycle checkpoints) in PAR, DTP, and DTEP cells. $n = 1$ biological replicate. See also Figure S1.

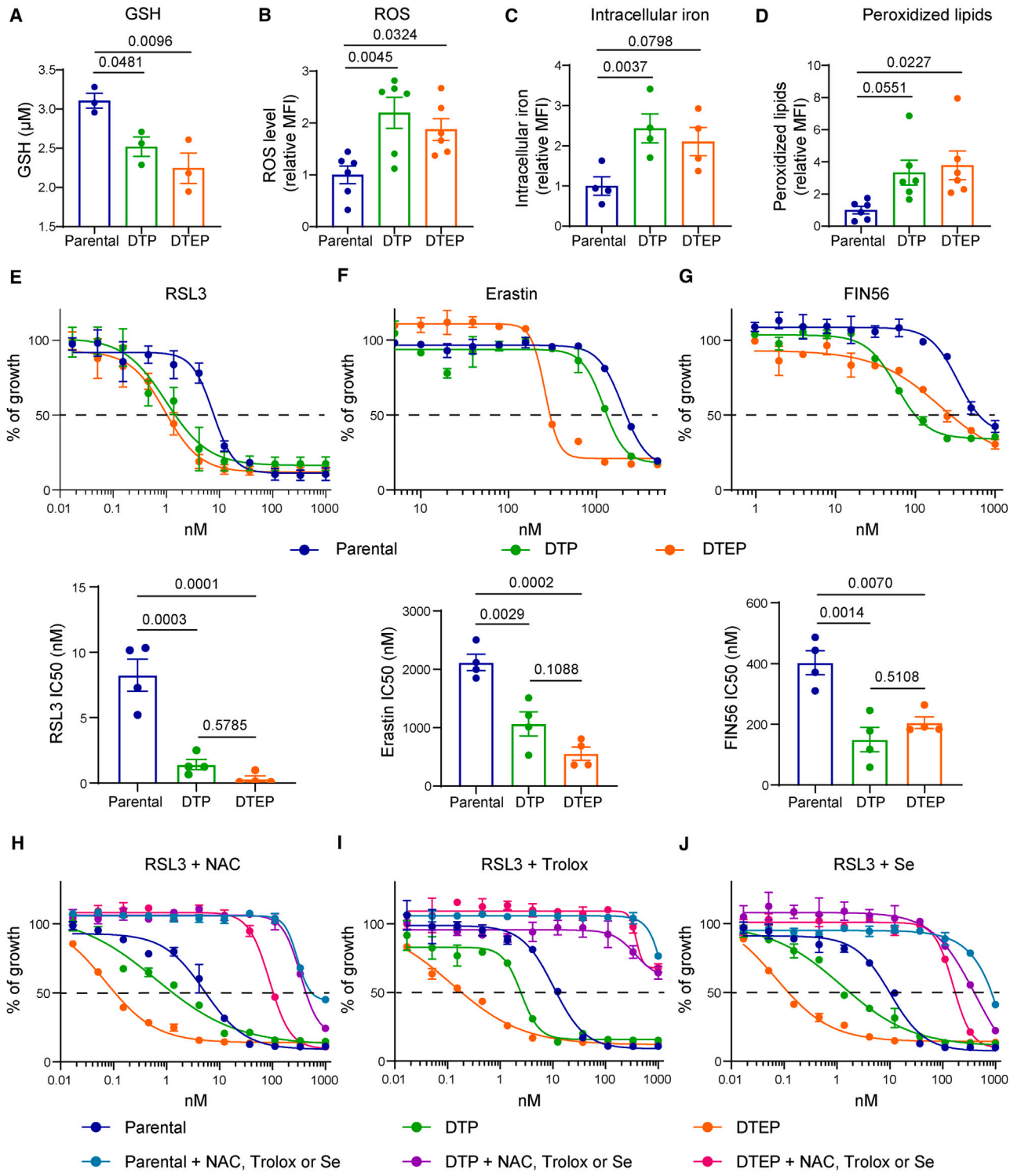

Figure 3. DTP and DTEP HCC364 cells are hypersensitive to ferroptosis induction *in vitro*

(A) Intracellular GSH concentration in parental, DTP, and DTEP HCC364 cells. *n* = 3 biological replicates.

(B) ROS level in parental, DTP, and DTEP HCC364 cells. *n* = 6 biological replicates.

(C) Iron level in parental, DTP, and DTEP HCC364 cells. *n* = 4 biological replicates.

(D) Peroxidized lipids content in parental, DTP, and DTEP HCC364 cells. *n* = 6 biological replicates.

(legend continued on next page)

To further evaluate the role of GPX4 in the adaptation to D/T in a more translational setting, we performed *in vivo* assays. To this end, we introduced the luciferase gene into the parental 1D-PDX cells before their implantation in the lungs of immunocompromised mice via direct lung injection (Figure 4D). D/T treatment was started when overt progression was observed resulting in significant disease control with approximately a 10-fold tumor burden reduction. Yet, the therapeutic response was transient and D/T-treated tumors slowly regained proliferative capacity indicative of progressive disease (Figure 4E). This feature was calculated following clinical criteria and was determined to occur when D/T-treated tumors reached a volume 20% higher to that estimated at the beginning of the drug treatment.[30] At this point, the disease progression cohort was split in two groups with one receiving the GPX4 inhibitor RSL3 as a next-line therapy. Remarkably, GPX4 inhibition of D/T-resistant tumors *in vivo* resulted in a 10-fold tumor growth reduction compared to the untreated cohort (Figures 4E–4G). Immunohistochemical staining of 4-hydroxynonenal (4-HNE) further confirmed the accumulation of lipid peroxides in lung tumors upon RSL3 treatment while GPX4 expression was comparable between the two groups (Figure 4H). These results suggest that the non-genetic adaptation to D/T therapy *in vivo* renders $BRAF^{V600E}$-mutant tumors vulnerable to ferroptosis triggers.

MAPK reactivation-mediated resistance and associated ROS vulnerabilities

Persister cells represent a reservoir from which acquired resistance eventually arises. In the context of D/T treatment, various bypass mutations including activating substitutions in *K*- and *NRAS* have been described in $BRAF^{V600E}$ lung tumors as potential mediators of clinical resistance.[4] In order to investigate whether RAS-mediated MAPK reactivation would also result in sensitivity to GPX4 inhibition and induction of ferroptosis, we took advantage of a D/T-resistant cell line (DFCI471) derived from a fresh biopsy at disease progression (Figures S6A–D). Sequencing of both the tumor and plasma revealed an $NRAS^{Q61K}$ mutation that co-existed with the $BRAF^{V600E}$ oncogene with no additional genomic alterations potentially linked to D/T resistance.[14] Indeed, short hairpin RNA-mediated NRAS knockdown decreased MAPK signaling and reverted the resistant phenotype (Figures S6E–S6H). These DFCI471 cells, unlike DTEPs from both HCC364 and 1D cells, turned out to be resistant to ferroptosis trigger erastin or the GPX4 inhibitor RSL3 (Figures 5A and 5B). To further confirm this result using another NRAS-dependent cellular model, we rescued the HCC364 DTPs by exogenous expression of $NRAS^{Q61K}$. Lentiviral delivery of the oncogene restored cell proliferation and induced D/T resistance increasing the IC50 of both compounds up to 50-fold (Figures S7A–S7C). This was correlated with the restoration of MAPK signaling and downstream transcriptional output to levels comparable to those of parental HCC364 cells (Figures S7D and S7E). In good agreement with the response of DFCI471 cells, the $HCC364^{NRAS}$ cells were insensitive to RSL3 or to erastin and displayed drug sensitivity values similar to those of the parental cells (Figures 5A and 5B). Interestingly, these phenotypes were replicated in another cellular setting in which D/T resistance occurred independently of acquired RAS mutations. We derived a spontaneous D/T-resistant HCC364 clone that displayed *EGFR* amplification (CNV 6.3), resulting in MAPK signaling and proliferation levels under D/T treatment similar to those of the untreated parental cells (Figures S7F–S7H). Furthermore, these $HCC364^{EGFRa}$ cells were insensitive to ferroptosis triggers (Figures 5A and 5B). These results suggest that in contrast to the persister state, acquired resistance to D/T driven by MAPK reactivation does not result in sensitivity to ferroptosis inducers.

We speculated that in this context of acquired resistance due to MAPK reactivation, GPX4 might not be a limiting redox factor since RAS/MAPK signaling has been shown to increase cellular GSH production by up-regulating the cystine/glutamate antiporter xCT.[31] Indeed, we found that DFCI471, $HCC364^{NRAS}$, and $HCC364^{EGFRa}$ cell lines displayed increased SLC7A11 mRNA and protein levels (Figures 5C and 5D). Accordingly, we went on to identify alternative actionable vulnerabilities that could be effective in the context of acquired resistance. A functionally equivalent *NRAS* mutation (Q61H) has been reported to mediate D/T insensitivity in $BRAF^{V600E}$-mutant melanoma cells.[8] In this tumor type, the resistant cells were treated with the histone deacetylase inhibitor (HDACi) vorinostat leading to reduced expression of SLC7A11 and elevation of oxidative stress to toxic levels.[8] Similarly, we found that DFCI471 cells treated with vorinostat or the related HDACi panobinostat triggered ROS production with a concomitant decrease in cell viability (Figures 5E and 5F). Treatment with the antioxidant NAC diminished the ROS production induced by both HDAC inhibitors and partly restored cell proliferation (Figures 5E and 5F). This illustrated the central role of oxidative stress as an acquired vulnerability following *NRAS*-mediated D/T resistance in $BRAF^{V600E}$-mutant LUAD. Similarly, HDACi treatment decreased the proliferation rate of both $HCC364^{NRAS}$ and $HCC364^{EGFRa}$ cells. This was again linked to ROS-dependent stress as co-treatment with NAC partly restored the growth rate of HDACi-treated cells (Figures 5F and S7I). In agreement with the pharmacologic approach, CRISPR-mediated ablation of SLC7A11 decreased the ability of these cells to grow in the presence of D/T (Figure S2).

Finally, we investigated whether HDACi could be applicable in a more clinically relevant setting. To this end, we took advantage of a second PDX-derived cell line (clone 1E).[29] In our hands, 1E-PDX cells became insensitive to D/T and displayed reactivated MAPK signaling as well as proliferation rates similar to those of the parental controls (Figures 6A–6C). Unlike the 1D-DTEPs (Figure 4A), D/T-resistant 1E cells (1E-R) maintained their high proliferative capacity following a drug holiday, suggesting that it may be mediated by a genetic alteration. Targeted sequencing analysis identified a *BRAF* gene amplification (CNV 15.4) compared

(E–G) Cell viability assessment by MTT assay of parental, DTP, and DTEP HCC364 cells treated with serial dilutions of RSL3 (E), erastin (F), or FIN56 (G) for 72 h (upper panel). IC50 values (lower panel) are represented for each condition. $n = 4$ biological replicates.

(H–J) Cell viability assessment by MTT assay of parental, DTP, and DTEP HCC364 cells treated with serial dilutions of RSL3 in the presence of 2.5 mM N-acetylcysteine (NAC, H), 10 μM Trolox (I), or 200 nM selenium (Se, J) for 72 h $n = 3$ biological replicates. All data were analyzed using one-way ANOVA followed by Dunnett's multiple comparisons post-test and are shown as the mean values ± SEM. See also Figures S2–S4 and S10.

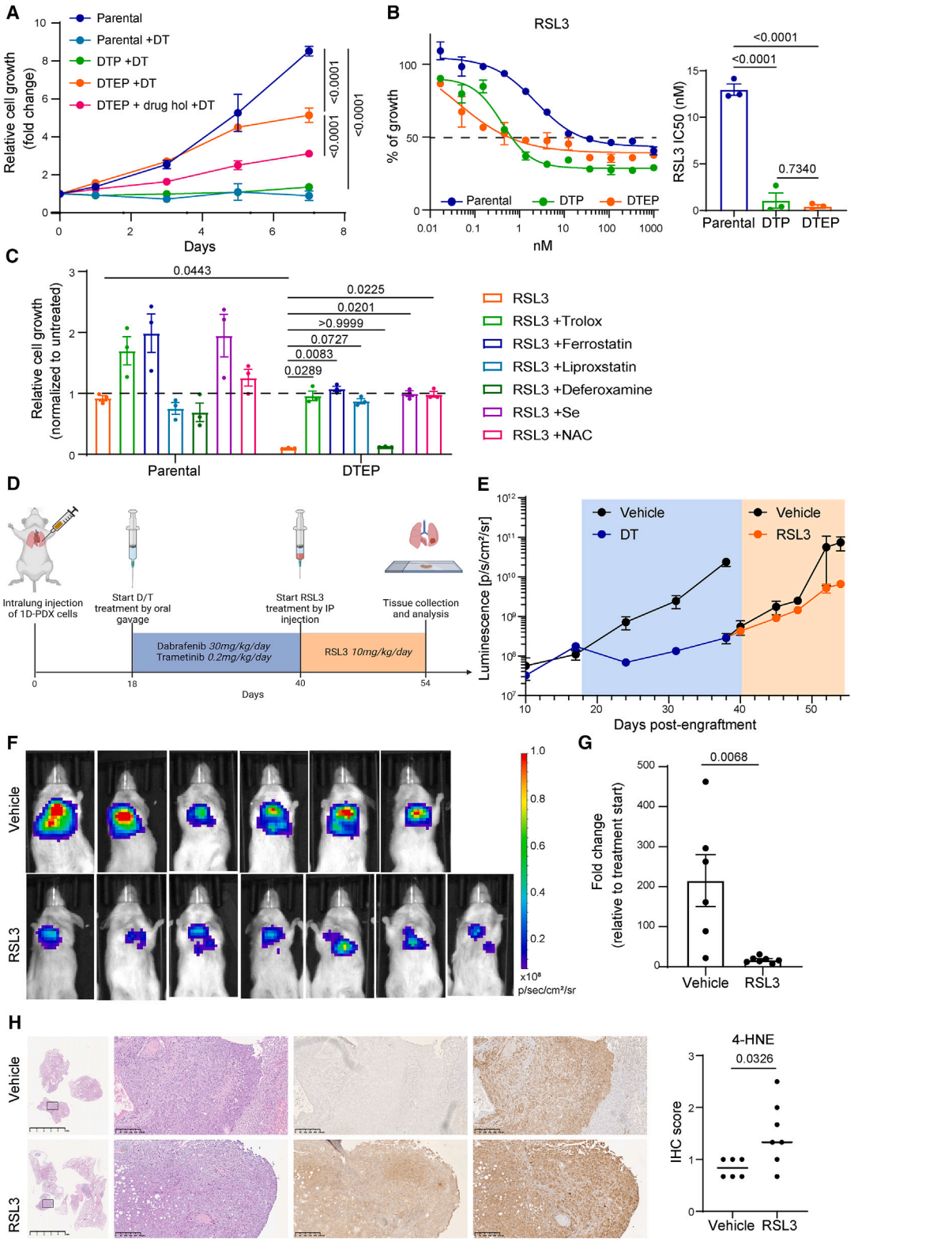

Figure 4. GPX4 inhibition reduces the tumor growth of D/T-resistant cells *in vivo*

(A) DTPs and DTEPs were generated by maintaining *BRAF*^{V600E}-mutant 1D-PDX cells on increasing concentrations of D/T treatment for 3 and 40 weeks, respectively. Growth curves of parental, DTP, and DTEP 1D cells in the presence of 250/5 nM D/T. DTEPs underwent a drug holiday for 3 weeks and were

(legend continued on next page)

to parental controls (CNV 2). This mechanism of genetic resistance has been previously described in *BRAF*^{V600E}-mutant melanoma.[32] Similarly to the previous examples of MAPK reactivation, 1E-R cultures displayed elevated SLC7A11 protein and mRNA levels (Figures 6B and 6D) as well as cystine uptake (Figure 6E). Likewise, 1E-R cells were insensitive to the ferroptosis triggers RSL3 and erastin (Figures S8A and S8B). Importantly, they showed increased sensitivity to HDACi treatment when compared to 1E-PDX parental cells in an oxidative stress-dependent manner (Figures 6F, S8C, and S8D).

Altogether, these results suggest that acquired resistance-mediated MAPK signaling reactivation results in both ROS toxicities and associated vulnerabilities that are mechanistically different from those observed during the non-genetic adaptation observed in DTEPs.

Targeting *NRAS*-dependent acquired resistance *in vivo*

We next investigated the therapeutic potential of the HDACi vorinostat and panobinostat on D/T-resistant LUAD *in vivo*. To this end, we used the DFCI471 model since RAS-mediated D/T resistance is frequent in the clinical setting.[4] DFCI471 xenografts were implanted and allowed to grow before treatment initiation (Figure 6G). Remarkably, exposure to the HDACi compounds induced a significant decrease in DFCI471 tumor growth that correlated with decreased levels of the proliferation marker phosphorylated histone H3 (Figures 6H and 6I). The higher therapeutic benefit observed with panobinostat may be due to increased HDAC inhibition *in vivo* as measured by acetylated H3 levels in tumor extracts (Figure 6J). In good agreement, panobinostat more efficiently reduced the expression levels of SLC7A11 potentially explaining its higher therapeutic effect (Figure 6J).

In sum, our results suggest that enhanced oxidative stress caused by HDACi might be a therapeutic vulnerability to treat *BRAF*^{V600E} D/T-resistant tumors due to acquired alterations leading to MAPK reactivation.

DISCUSSION

Most targeted therapies have limited efficacy when applied as single-agent treatments due to the rapid onset of drug resistance. When possible, improved regimens have been implemented in the clinic by applying rational drug combinations. BRAF-mutant LUAD has been one of these cases as demonstrated by a recent study reporting superior 5-year survival rates in a non-comparative phase 2 trial evaluating single vs. combined D/T therapy.[5] Unfortunately, even if administered as combination regimens, tumor progression eventually unfolds, leaving drug-insensitive patients with limited therapeutic alternatives.[4] Several mechanisms driving resistance to D/T have been identified in relapsing BRAF-mutant patients (mostly in the context of melanoma), often resulting in MAPK reactivation or increased signaling through parallel and downstream pathways such as PI3K or Hippo/Yap, respectively. Regarding BRAF-mutant LUAD, these resistance mechanisms have only been documented in a few case reports.[6,7,12,13,16] Such heterogeneous clinical landscape complicates the anticipation of potential treatments to overcome disease progression. In this context, the identification of targetable molecular vulnerabilities that could be utilized to fight the onset of acquired resistance is a pressing medical need.

Accumulating evidence suggests that DTPs are the cellular reservoir that eventually leads to fully resistant disease upon additional acquired modifications.[21,22,33] Irrespective of whether DTPs are rare pre-existing entities in the primary tumor, drug-induced, or the result of stochastic reprogramming, eradicating DTPs could be of great therapeutic value. Yet, while efficacious therapeutic approaches have yet to be established, a number of potential vulnerabilities have been identified in DTPs.[33] Among those, up-regulation of antioxidant responses is linked with the persister phenotype in multiple cancer types.[34–37] Also, a recent report demonstrated that NPC1L1-mediated uptake of vitamin E was increased in DTPs and its inhibition by ezetimibe had a significant anti-tumor effect in a pre-clinical cancer model.[38] Interestingly, metabolic reprogramming through adaptation of both mitochondrial respiration and lipid metabolism has been shown to be a key mediator of resistance to MAPK inhibitors in BRAF-mutant melanoma.[39–42] Further investigations will determine whether, as suggested by the results presented here, targeting these altered metabolic pathways (only identified in the context of melanoma) could also represent an effective therapeutic strategy to overcome resistance in BRAF-mutated LUAD.

rechallenged with D/T to further confirm the non-genetic adaptation of these cells to the treatment (DTEP + drug hol + D/T). Data were analyzed using two-way ANOVA followed by Tukey's multiple comparisons post-test and are shown as the mean values ± SEM. n = 3 biological replicates.

(B) Cell viability assessment by MTT assay of parental, DTP, and DTEP 1D cells treated with serial dilutions of RSL3 for 72 h. Data are shown as the mean values ± SEM. IC50 values ± SD are indicated for each condition. n = 3 biological replicates.

(C) Cell viability assessment by MTT assay of parental and DTEP 1D cells treated with 50 nM RSL3 in the presence of 10 μM Trolox, 200 nM ferrostatin, 100 nM liproxstatin, 1 μM deferoxamine, 200 nM Se, or 2.5 mM NAC for 72 h. Data are normalized to untreated cells and shown as the mean values ± SEM. Data were analyzed using two-way ANOVA followed by Tukey's multiple comparisons post-test. n = 3 biological replicates.

(D) Schematic outline of the 1D intrapulmonary xenograft model. After lung orthotopic injection, mice were treated with dabrafenib (30 mg/kg/day) and trametinib (0.2 mg/kg/day) by oral gavage 5 days per week. At disease progression, mice were treated with RSL3 (10 mg/kg/day) by intraperitoneal injection 5 days per week. Mice were sacrificed and lungs were collected for further analysis.

(E) Follow-up of intralung 1D tumor growth by bioluminescence imaging. Mice were treated as mentioned in D. Data are represented as mean signal intensity (p/s/cm^2/sr) ± SEM, n = 6 or 7 mice for each group.

(F) Representative images of bioluminescence signal in mice treated with RSL3.

(G) Fold change in tumor growth compared to baseline (the start of RSL3 treatment, day 40 post-implantation) for individual cell xenografts treated for 14 days with vehicle or with 10 mg/kg/day RSL3. Fold changes were calculated based on the values presented in Figure 4E (p/s/cm^2/sr). Statistical significance was tested using unpaired two-tailed t test. n = 6 or 7 mice for each group.

(H) Representative 4-HNE and GPX4 immunostaining in lung sections of mice treated with RSL3. Quantification of 4-HNE staining scores in 1D tumors from mice treated with vehicle or with RSL3. Data are shown as mean scores (average of three independent stainings) per mice and were analyzed using Mann-Whitney t test. n = 6 or 7 mice for each group. See also Figures S1 and S9.

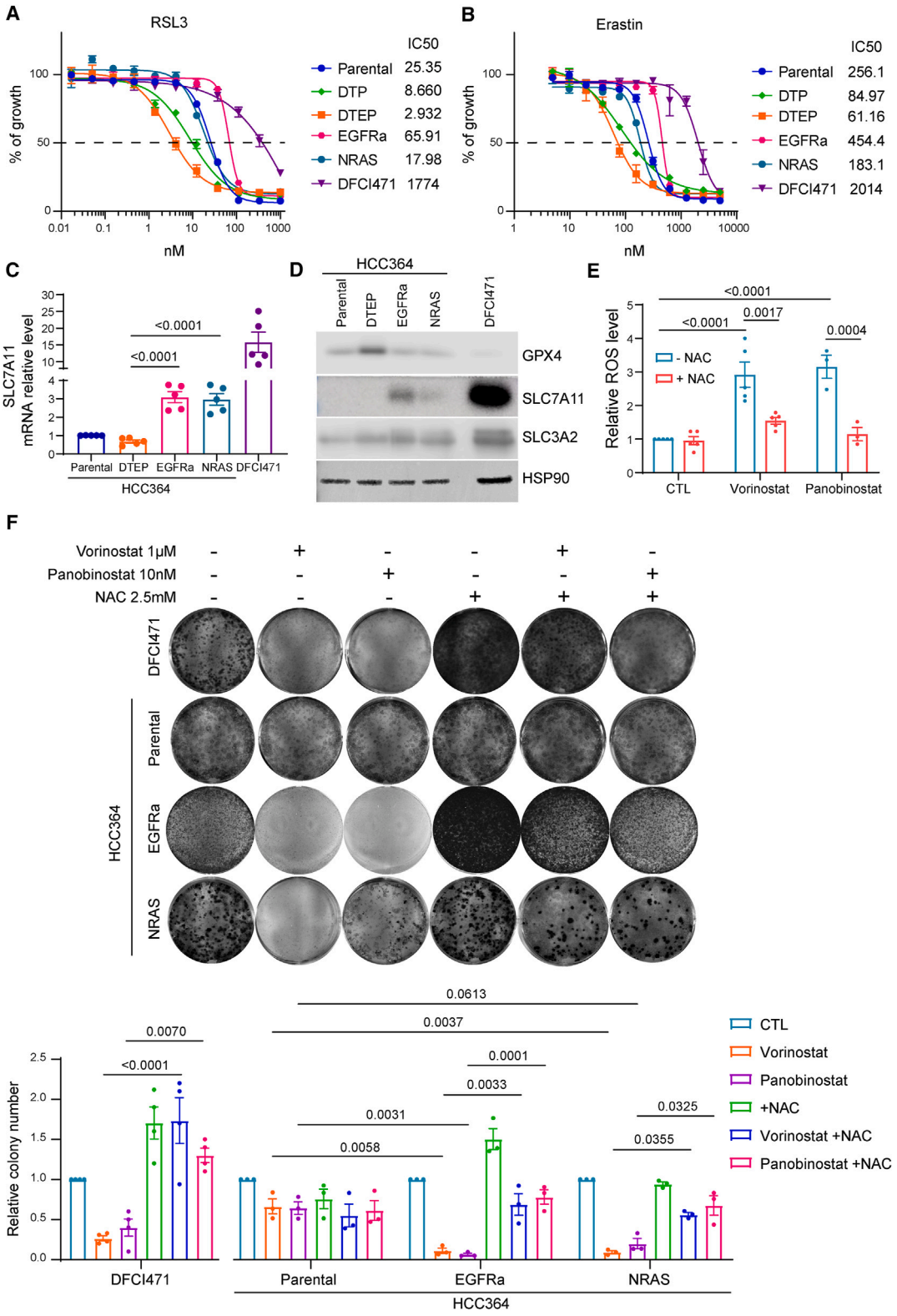

Figure 5. *NRAS*-mediated resistance leads to increased sensitivity to oxidative stress but not to ferroptosis

(A and B) DFCI471 cells derived from a biopsy of a patient with *BRAF*^{V600E} LUAD at disease progression upon D/T treatment. HCC364^{NRAS} cells were generated by exogenous expression of NRAS^{Q61K} in HCC364-DTPs and HCC364^{EGFRa} cells were derived spontaneously from HCC364-DTEPs after continuous D/T (250/

(legend continued on next page)

In this context, our genome-wide genetic screen identified the lipid hydroperoxidase GPX4 as a top candidate required by *BRAF*-mutant lung cancer cells to survive D/T treatment (Figure 1). Indeed, GPX4 has been previously identified as a key mediator to sustain the DTP cell state in various tumor types.[17,18,43] Our findings using *BRAF*^{V600E} PDX-derived lung cancer cell lines suggest that GPX4 inhibition *in vivo* at the time of early relapse on D/T treatment (based on RECIST criteria) results in significant disease control (Figures 4E–4G). Importantly, a pleural effusion sample obtained from a patient with metastatic LUAD who initially responded to D/T displayed extensive signs of lipid peroxidation (identified by 4-HNE staining) at the time of early disease progression that was absent in the pre-treatment diagnostic samples (Figure 7). This result suggests that GPX4 inhibitors and/or other ferroptosis-inducing treatments could represent an alternative line of treatment when early signs of disease progression are detected. Admittedly, it is currently unclear at what point of disease progression the acquired resistance takes over adaptive drug tolerance. Recent results at the single-cell level have demonstrated that the DTP state is in part conserved at the early resistant setting.[26] Our transcriptional data *in vitro* and, more importantly, the response of PDX to GPX4 inhibitors and the identification of lipid peroxidation markers in a patient biopsy reinforce this hypothesis. Altogether, we believe that this evidence is clinically relevant since patients with *BRAF*^{V600E} mutant progressing on D/T would undergo treatment discontinuation followed by chemoimmunotherapy or immunotherapy alone, if PD-L1 expression is equal or higher than 50%, with relatively modest efficacy.[44] Unfortunately, GPX4 inhibition failed to up-regulate immune checkpoint proteins both *in vitro* and *in vivo* (Figure S9), as this might have provided a potential synergistic effect with immunotherapy. Nevertheless, novel compounds with reduced toxicity should be developed in order to consider GPX4 inhibition or alternative ferroptosis triggers a realistic clinical option. In any case, our data, together with pre-existing evidence, reinforce the existence of targetable redox vulnerabilities during the DTP state that could have future clinical applicability.

Further supporting the increased susceptibility to ferroptosis following D/T treatment, iron levels are also elevated in DTP and DTEP populations as evidenced by increased ferritin and stable transferrin receptor (TFRC) levels (Figure S10). Although it may seem counterintuitive that cells undergoing oxidative cells stress would up-regulate iron metabolism, this is consistent with the increased dependency of DTP cells on iron-sulfur cluster (ISC) biosynthesis. Indeed, ISC biosynthesis is a significant characteristic of sensitivity in DTPs, as evidenced by their dependency on various ISC assembly factors that appeared as drop-out hits in the genetic screen (Figure 1). Importantly, ISC availability is emerging as a major regulator of ferroptosis sensitivity, with ISC triggering an iron starvation response,[45] leading to increased iron uptake and iron mobilization via ferritin degradation, thereby predisposing to ferroptosis.[46] At the mitochondrial level, ISC availability is also required for proper regulation of GSH availability, suggesting a potential interaction between ISC availability and GSH dynamics. Further analyses will be required to identify the molecular mechanisms that result in increased ISC dependency.

Finally, our results also demonstrate that ferroptosis activators, that show therapeutic efficacy in the persister stage, display reduced anti-tumor efficacy once resistance mechanisms that reactivate MAPK signaling have been acquired. This may be due to the fact that RAS/MAPK signaling directly activates the expression and activity of the cystine/glutamate antiporter xCT.[31] Of note, the SLC7A11 subunit of the antiporter is overexpressed in patients with *KRAS*-mutant LUAD and its inhibition leads to prolonged survival.[47] Imported cystine is then reduced to cysteine providing a rate-limiting substrate for the cellular GSH synthesis and increased antioxidant power. In addition, RAS signaling also inhibits ferroptotic death by up-regulating the ferroptosis suppressor protein 1.[48] In sum, in the context of MAPK signaling reactivation, GPX4 is unlikely to be a limiting redox factor thus reducing the therapeutic effect of direct inhibitors or other ferroptosis triggers as described in this manuscript. Indeed, recent evidence suggests that redox metabolism is a crucial function in DTP and DTEP lung cancer populations and its control is exerted at multiple levels.[49] This complex and still incompletely characterized network of anti-oxidative functions potentially offers various options with therapeutic potential to increase ROS levels to a lethal threshold in these cellular populations. Some of these options, such as the recently reported BET inhibition,[49] may be better tolerated than the ferroptosis triggers described here.

Nevertheless, we have observed that acquired resistance due to MAPK reactivation also results in ROS-dependent vulnerabilities mechanistically different from those observed in the DTP stage. We have confirmed elevated SLC7A11 expression levels and cystine uptake in PDX-derived lung cancer D/T-resistant cell lines with either an *NRAS*-activating mutation, EGFR amplification, or copy-number gain of the *BRAF*^{V600E} driver (Figures 5C, 5D, 6B, 6D, and 6E). Treatment of these resistant cells with HDAC inhibitors significantly reduced their viability in

5 nM) treatment for 70 weeks. Cell viability assessment by MTT assay of parental and DTEP HCC364, HCC364^{EGFRa}, HCC364^{NRAS}, and DFCI471 cells treated with serial dilutions of RSL3 (A) or erastin (B) for 72 h. Data are shown as the mean values ± SEM. $n = 3$ biological replicates.

(C) Quantitative reverse-transcription PCR (RT-PCR) analysis of relative *SLC7A11* mRNA level in parental and DTEP HCC364, HCC364^{EGFRa}, HCC364^{NRAS}, and DFCI471 cells. Data were analyzed using one-way ANOVA followed by Tukey's multiple comparisons post-test and are shown as the mean values ± SEM. $n = 5$ biological replicates.

(D) Immunoblot of SLC7A11, SLC3A2, and GPX4 in parental and DTEP HCC364, HCC364^{EGFRa}, HCC364^{NRAS}, and DFCI471 cells. HSP90 was used as a loading control. $n = 3$ biological replicates.

(E) Intracellular ROS level in DFCI471 cells co-treated with 1 μM vorinostat or 10 nM panobinostat and 2.5 mM NAC for 72 h. Data were analyzed using two-way ANOVA followed by Tukey's multiple comparisons post-test and are shown as the mean values ± SEM. $n = 3$ or 5 biological replicates.

(F) Clonogenic assay of DFCI471, HCC364, HCC364^{EGFRa}, and HCC364^{NRAS} cells co-treated with 1 μM vorinostat or 10 nM panobinostat and 2.5 mM NAC. Data were analyzed using two-way ANOVA followed by Tukey's multiple comparisons post-test and are shown as the mean values ± SEM. $n = 3$ biological replicates. See also Figures S2, S6, S7, and S10.

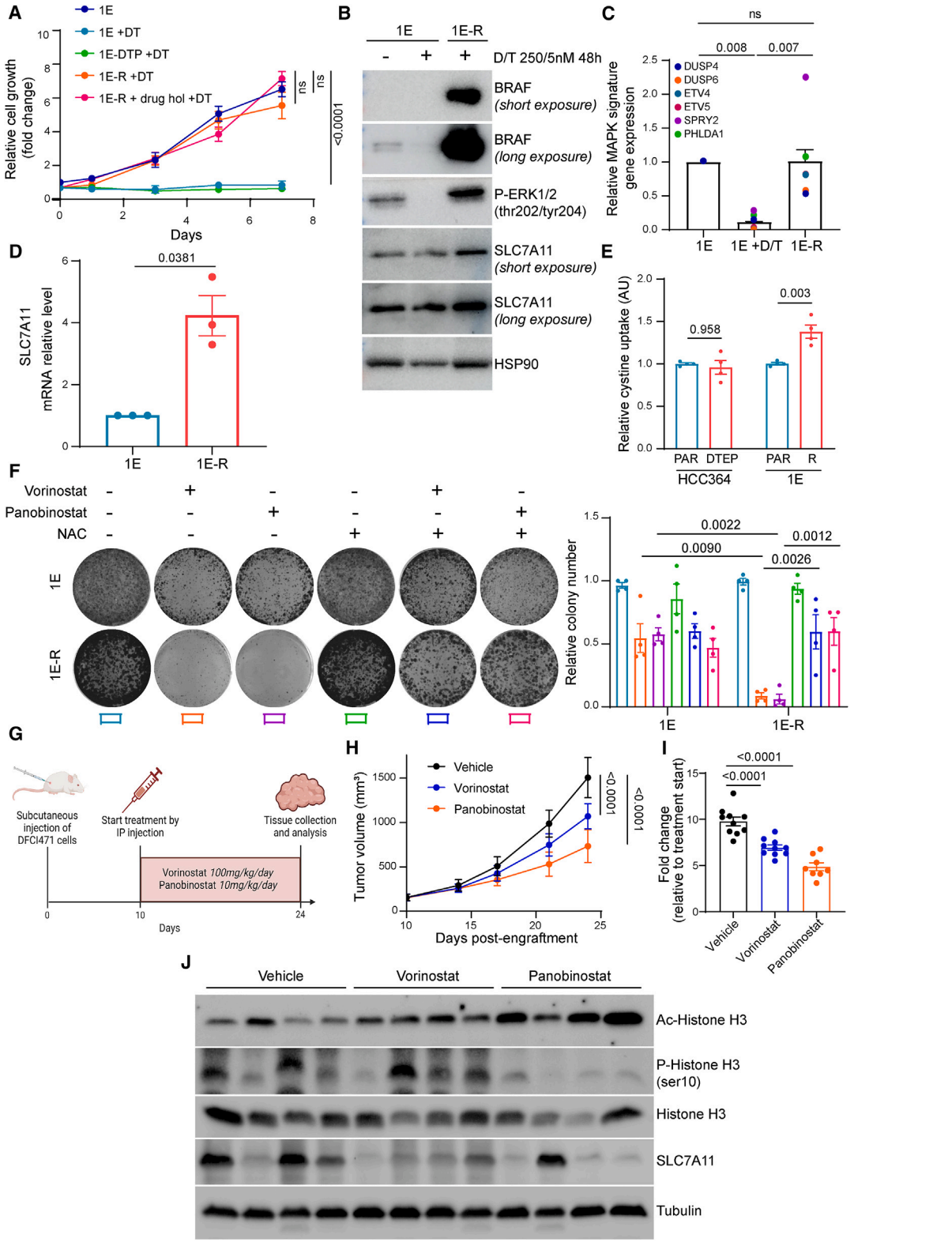

(legend on next page)

an ROS-dependent manner (Figures 5F and 6G–6I). Furthermore, this treatment resulted in a 3-fold decrease in tumor progression *in vivo*. This is in good agreement with previous findings in D/T-resistant *BRAF*^{V600E}-mutant melanoma harboring an *NRAS* mutation.[8] However, as previously reported in this tumor context, HDAC inhibitors display ROS-independent effects on cancer cells,[8] and it is therefore likely that the therapeutic benefit described here in LUAD is not entirely dependent on the control of the XCt antiporter. Yet, supported by several pre-clinical works,[8,50–53] a phase 1/2 clinical trial (NCT02836548) has been initiated to evaluate vorinostat for the treatment of patients with *BRAF*^{V600E}-mutant advanced melanoma progressing on D/T treatment.[54] Preliminary results were recently reported demonstrating that intermittent vorinostat treatment elicited durable anti-tumor responses in a subset of patients accompanied by the elimination of MAPK reactivating mutations when evaluated by ctDNA.[55] The termination of this study will potentially confirm its anti-tumor efficacy previously anticipated in the pre-clinical setting.[35] It may also inform of its potential applicability to other *BRAF*-mutant tumor types progressing on D/T inhibitor therapy due to acquired mutations leading to MAPK reactivation.

Limitations of the study

Our work identifies two redox-related cellular states as sequential treatment vulnerabilities to enhance the response of *BRAF*^{V600E}-mutant lung cancer to D/T combination therapy. Defining the most sensitive windows to GPX4 and HDAC inhibitors that would maximize therapeutic benefit remains a critical point. Evidence from our *in vivo* models and from an index patient undergoing D/T treatment suggests some extent of overlapping that could in part be due to the transition nature of the DTEPs. The absence of *bona fide* DTP and DTEP markers *in vivo* together with the lack of robust longitudinal sampling during D/T treatment further complicates the definition of precise temporary regimens based on these findings. Furthermore, novel GPX4 inhibitors with enhanced pharmacodynamics properties should be developed. In sum, future studies are mandatory to explore the effectiveness of these stage-specific treatments across a broader spectrum of *BRAF*^{V600E}-mutant lung cancer models.

STAR★METHODS

Detailed methods are provided in the online version of this paper and include the following:

- KEY RESOURCES TABLE
- RESOURCE AVAILABILITY
  - Lead contact
  - Materials availability
  - Data and code availability
- EXPERIMENTAL MODEL AND STUDY PARTICIPANT DETAILS
  - Cell lines and cell culture
  - Animals and *in vivo* studies
  - Patient sample
- METHOD DETAILS
  - shRNA-mediated NRAS knock-down
  - GPX4 and SLC7A11 inducible CRISPR-Cas9 Knock-out
  - Genome-wide sgRNA library construction
  - CRISPR/Cas9 screening for determinants of dabrafenib/trametinib sensitivity
  - CRISPR/cas9 screening data analysis
  - RNA-sequencing and data analysis
  - GSH measurement
  - ROS measurement
  - Intracellular iron measurement
  - Peroxidized lipids content measurement
  - Cell growth assay
  - Clonogenic assay
  - Apoptosis assay
  - Immunohistochemistry
  - Somatic variants analysis
  - Cystine uptake
  - Western blotting
  - RNA extraction, reverse transcription and quantitative PCR (RT-qPCR)
- QUANTIFICATION AND STATISTICAL ANALYSIS

Figure 6. MAPK pathway reactivation through *BRAF* amplification is associated with ROS vulnerabilities and *in vivo* targeting of *NRAS*-mediated D/T resistance in *BRAF*^{V600E} LUAD cells with HDAC inhibitors

(A) DTPs and 1E-R cells were generated by maintaining *BRAF*^{V600E}-mutant 1E-PDX cells on increasing concentrations of D/T treatment for 3 and 30 weeks, respectively. Growth curves of parental, DTP, and -R 1E cells in the presence of 250/5 nM D/T. 1E-R cells underwent a drug holiday for 3 weeks and were rechallenged with D/T to confirm the genetic adaptation of these cells to the treatment (1E-R + drug hol + D/T). Data were analyzed using two-way ANOVA followed by Tukey's multiple comparisons post-test and are shown as the mean values ± SEM. *n* = 3 biological replicates.

(B) Immunoblot of BRAF, phospho-ERK (p-ERK), and SLC7A11 in 1E and 1E-R cells cultured in the presence of 250/5 nM D/T for 48 h. HSP90 was used as a loading control. *n* = 2 biological replicates.

(C) Quantitative RT-PCR analysis of relative MAPK pathway target genes (*DUSP4*, *DUSP6*, *ETV4*, *ETV5*, *SPRY2*, and *PHLDA1*) mRNA levels in 1E and 1E-R cells cultured in the presence of 250/5 nM D/T for 48 h. Data were analyzed using one-way ANOVA followed by Tukey's multiple comparisons post-test and are shown as the mean values ±SEM. *n* = 3 biological replicates.

(D) Quantitative RT-PCR analysis of *SLC7A11* mRNA level in 1E and 1E-R cells. Data were analyzed using unpaired t test with Welch's correction and are shown as the mean values ± SEM. *n* = 3 biological replicates.

(E) Intracellular cystine uptake in HCC364 (parental and DTEP) and 1E (parental and -R) cells. Data were analyzed using two-way ANOVA followed by Tukey's multiple comparisons post-test and are shown as the mean values ± SEM. *n* = 4 biological replicates.

(F) Clonogenic assay of 1E and 1E-R cells co-treated with 1 μM vorinostat or 10 nM panobinostat and 2.5 mM NAC. Data were analyzed using two-way ANOVA followed by Tukey's multiple comparisons post-test and are shown as the mean values ± SEM. *n* = 4 biological replicates.

(G) Schematic outline of the DFCI471 subcutaneous xenograft model. Mice were treated with vorinostat (100 mg/kg/day) or panobinostat (10 mg/kg/day) by intraperitoneal injection 5 days per week. After 14 days, mice were sacrificed and tumors were collected for further analysis.

(H) Follow-up of tumor growth of the indicated conditions. Data are represented as mean tumor volume ±SEM. *n* = 8 or 10 mice for each group.

(I) Fold change in tumor growth compared to baseline.

(J) Immunoblot of acetyl and phospho-histone H3 (Ac and p-histone H3), histone H3, and SLC7A11 in 4 representative tumors per condition. Tubulin was used as a loading control. *n* = 4 biological replicates. See also Figure S8.

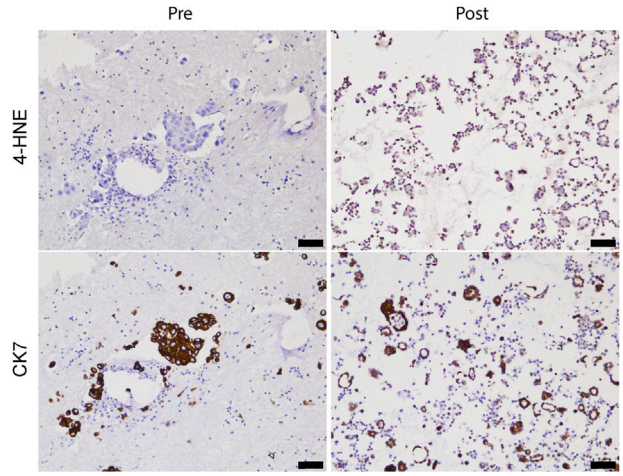

Figure 7. Clinical evidence of the occurrence of lipid peroxidation at disease progression following D/T treatment

Representative 4-HNE immunostaining in patient samples pre- and post-D/T treatment. Immunostaining for the epithelial marker CK7 was performed in consecutive sections as control. Scale bars represent 75 μm.

SUPPLEMENTAL INFORMATION

Supplemental information can be found online at https://doi.org/10.1016/j.xcrm.2024.101663.

ACKNOWLEDGMENTS

Research in D.S. laboratory was funded by Siric-BRIO (Bordeaux Recherche Intégrée en Cancérologie, INCa convention 2018-006 and INSERM convention 18CI05500) and a Senior Chair Idex-Université de Bordeaux (2016-0396) and grants from Institut National Du Cancer (INCA_13911), Ministerio de Ciencia e Innovación (Retos PID2020-116824RB-I00), and by AECC Excellence Program 2022 (EPAEC222641CICS). M.-J.N. was supported by postdoctoral fellowships from Fondation ARC pour la recherche contre le cancer and from FNRS-Télévie. This work was also supported by the Fund André Daners, managed by the King Baudouin Foundation and by the Foundation Leon Fredericq. A.V. received funding from ISCIII (grant PI22-00548, co-funded by FEDER). E.N. received funding from ISCIII (grant PI21/00789, co-funded by FEDER). C.A. received funding by the Giovanni Armenise-Harvard Foundation, the Italian Ministry of University and Research (FARE-R207ENY9KZ), the European Research Council (ERC) under the European Union's Horizon 2020 research and innovation program (grant 101001288), and AIRC under IG 2021-ID. 25737 project. The authors are thankful to Mrs. F. Perin and A. Demanche for expert technical assistance. We acknowledge the technology platforms of the GIGA at University of Liege: animal, imaging/flow cytometry, and viral vector facilities. The authors also thank the Animalerie A2 (Bordeaux University) for excellent assistance and CRISP'edit and Vect'UB facilities (TBMCore UAR CNRS3427, Inserm US05, Bordeaux University) for help with library packaging into lentiviral particles and CRISPR experiments and analysis. The schemes were created with BioRender.com.

AUTHOR CONTRIBUTIONS

M.-J.N., C.A., and D.S. conceived this project and designed the study. M.-J.N., E.D., E.R., S.S.J., V.P.-M., B.T., L.G., R.C., V.V., B.K., F.L., J.H., A.V., and M.H. performed the experiments and analyzed the data. S.d.H., J.Y.X., B.S., E.Z., A.B., D.C., O.C., P.L., P.A.J., B.R., and M.A. provided materials, methodological support, and/or conceptual advice. M.-J.N., P.P., E.N., B.R., C.A., and D.S. wrote the manuscript. All authors discussed the results and commented on the manuscript.

DECLARATION OF INTERESTS

D.S. received research fees from Aelin Therapeutics. C.A. received research fees from Revolution Medicines, Aelin Therapeutics, Verastem, Roche, and Boehringer Ingelheim. E.N. reports research funding from Pfizer and Roche. P.L. is listed as an inventor on patent applications filed by MSKCC that describe approaches to treat KRAS or BRAF-mutant tumors. P.A.J. has received consulting fees from AstraZeneca, Boehringer Ingelheim, Pfizer, Roche/Genentech, Takeda Oncology, ACEA Biosciences, Eli Lilly and Company, Araxes Pharma, Ignyta, Mirati Therapeutics, Novartis, Loxo Oncology, Daiichi Sankyo, Sanofi Oncology, Voronoi, SFJ Pharmaceuticals, Takeda Oncology, Transcenta, Silicon Therapeutics, Syndax, Nuvalent, Bayer, Eisai, Biocartis, Allorion Therapeutics, Accutar Biotech, Monte Rosa, Scorpion Therapeutics, Merus, Frontier Medicines, Hongyun Biotechnology, Duality, and AbbVie; post-marketing royalties from DFCI-owned intellectual property on EGFR mutations licensed to Lab Corp; sponsored research agreements with AstraZeneca, Daiichi Sankyo, Puma, Boehringer Ingelheim, Eli Lilly and Company, Revolution Medicines, and Astellas Pharmaceuticals; and stock ownership in Gatekeeper Pharmaceuticals. M.M.A. reports grants and personal fees from Genentech, grants and personal fees from Bristol Myers Squibb, personal fees from Merck, grants and personal fees from AstraZeneca, grants from Lilly, and personal fees from Maverick, Blueprint Medicine, Syndax, Ariad, Nektar, Gritstone, ArcherDX, Mirati, NextCure, Novartis, EMD Serono, and Panvaxal/NovaRx, outside the submitted work.

Received: July 3, 2023
Revised: May 22, 2024
Accepted: July 8, 2024
Published: August 1, 2024

REFERENCES

1. Lavoie, H., and Therrien, M. (2022). Structural keys unlock RAS-MAPK cellular signalling pathway. Nature *609*, 248–249. https://doi.org/10.1038/d41586-022-02189-7.
2. Wiesweg, M., Preuss, C., Roeper, J., Metzenmacher, M., Eberhardt, W., Stropiep, U., Wedeken, K., Reis, H., Herold, T., Darwiche, K., et al. (2021). BRAF mutations and BRAF mutation functional class have no negative impact on the clinical outcome of advanced NSCLC and associate with susceptibility to immunotherapy. Eur. J. Cancer *149*, 211–221. https://doi.org/10.1016/j.ejca.2021.02.036.
3. Dagogo-Jack, I., Martinez, P., Yeap, B.Y., Ambrogio, C., Ferris, L.A., Lydon, C., Nguyen, T., Jessop, N.A., Iafrate, A.J., Johnson, B.E., et al. (2019). Impact of BRAF Mutation Class on Disease Characteristics and Clinical Outcomes in BRAF-mutant Lung Cancer. Clin. Cancer Res. *25*, 158–165. https://doi.org/10.1158/1078-0432.CCR-18-2062.
4. Tabbo, F., Pisano, C., Mazieres, J., Mezquita, L., Nadal, E., Planchard, D., Pradines, A., Santamaria, D., Swalduz, A., Ambrogio, C., et al. (2022). How far we have come targeting BRAF-mutant non-small cell lung cancer (NSCLC). Cancer Treat Rev. *103*, 102335. https://doi.org/10.1016/j.ctrv.2021.102335.
5. Planchard, D., Besse, B., Groen, H.J.M., Hashemi, S.M.S., Mazieres, J., Kim, T.M., Quoix, E., Souquet, P.J., Barlesi, F., Baik, C., et al. (2022). Phase 2 Study of Dabrafenib Plus Trametinib in Patients With BRAF V600E-Mutant Metastatic NSCLC: Updated 5-Year Survival Rates and Genomic Analysis. J. Thorac. Oncol. *17*, 103–115. https://doi.org/10.1016/j.jtho.2021.08.011.
6. Facchinetti, F., Lacroix, L., Mezquita, L., Scoazec, J.Y., Loriot, Y., Tselikas, L., Gazzah, A., Rouleau, E., Adam, J., Michiels, S., et al. (2020). Molecular mechanisms of resistance to BRAF and MEK inhibitors in BRAF(V600E) non-small cell lung cancer. Eur. J. Cancer *132*, 211–223. https://doi.org/10.1016/j.ejca.2020.03.025.
7. Ortiz-Cuaran, S., Mezquita, L., Swalduz, A., Aldea, M., Mazieres, J., Leonce, C., Jovelet, C., Pradines, A., Avrillon, V., Chumbi Flores, W.R., et al. (2020). Circulating Tumor DNA Genomics Reveal Potential

Mechanisms of Resistance to BRAF-Targeted Therapies in Patients with BRAF-Mutant Metastatic Non-Small Cell Lung Cancer. Clin. Cancer Res. *26*, 6242–6253. https://doi.org/10.1158/1078-0432.CCR-20-1037.

8. Wang, L., Leite de Oliveira, R., Huijberts, S., Bosdriesz, E., Pencheva, N., Brunen, D., Bosma, A., Song, J.Y., Zevenhoven, J., Los-de Vries, G.T., et al. (2018). An Acquired Vulnerability of Drug-Resistant Melanoma with Therapeutic Potential. Cell *173*, 1413–1425.e14. https://doi.org/10.1016/j.cell.2018.04.012.

9. Doench, J.G., Fusi, N., Sullender, M., Hegde, M., Vaimberg, E.W., Donovan, K.F., Smith, I., Tothova, Z., Wilen, C., Orchard, R., et al. (2016). Optimized sgRNA design to maximize activity and minimize off-target effects of CRISPR-Cas9. Nat. Biotechnol. *34*, 184–191. https://doi.org/10.1038/nbt.3437.

10. Winter, J., Schwering, M., Pelz, O., Rauscher, B., Zhan, T., Heigwer, F., and Boutros, M. (2017). CRISPRAnalyzeR: Interactive analysis, annotation and documentation of pooled CRISPR screens. Preprint at bioRxiv, 109967. https://doi.org/10.1101/109967.

11. Sanchez-Burgos, L., Navarro-Gonzalez, B., Garcia-Martin, S., Sirozh, O., Mota-Pino, J., Fueyo-Marcos, E., Tejero, H., Anton, M.E., Murga, M., Al-Shahrour, F., and Fernandez-Capetillo, O. (2022). Activation of the integrated stress response is a vulnerability for multidrug-resistant FBXW7-deficient cells. EMBO Mol. Med. *14*, e15855. https://doi.org/10.15252/emmm.202215855.

12. Nokin, M.J., Ambrogio, C., Nadal, E., and Santamaria, D. (2021). Targeting Infrequent Driver Alterations in Non-Small Cell Lung Cancer. Trends Cancer *7*, 410–429. https://doi.org/10.1016/j.trecan.2020.11.005.

13. Wang, V.E., Xue, J.Y., Frederick, D.T., Cao, Y., Lin, E., Wilson, C., Urisman, A., Carbone, D.P., Flaherty, K.T., Bernards, R., et al. (2019). Adaptive Resistance to Dual BRAF/MEK Inhibition in BRAF-Driven Tumors through Autocrine FGFR Pathway Activation. Clin. Cancer Res. *25*, 7202–7217. https://doi.org/10.1158/1078-0432.CCR-18-2779.

14. Abravanel, D.L., Nishino, M., Sholl, L.M., Ambrogio, C., and Awad, M.M. (2018). An Acquired NRAS Q61K Mutation in BRAF V600E-Mutant Lung Adenocarcinoma Resistant to Dabrafenib Plus Trametinib. J. Thorac. Oncol. *13*, e131–e133. https://doi.org/10.1016/j.jtho.2018.03.026.

15. Niemantsverdriet, M., Schuuring, E., Elst, A.T., van der Wekken, A.J., van Kempen, L.C., van den Berg, A., and Groen, H.J.M. (2018). KRAS Mutation as a Resistance Mechanism to BRAF/MEK Inhibition in NSCLC. J. Thorac. Oncol. *13*, e249–e251. https://doi.org/10.1016/j.jtho.2018.07.103.

16. Lin, L., Sabnis, A.J., Chan, E., Olivas, V., Cade, L., Pazarentzos, E., Asthana, S., Neel, D., Yan, J.J., Lu, X., et al. (2015). The Hippo effector YAP promotes resistance to RAF- and MEK-targeted cancer therapies. Nat. Genet. *47*, 250–256. https://doi.org/10.1038/ng.3218.

17. Hangauer, M.J., Viswanathan, V.S., Ryan, M.J., Bole, D., Eaton, J.K., Matov, A., Galeas, J., Dhruv, H.D., Berens, M.E., Schreiber, S.L., et al. (2017). Drug-tolerant persister cancer cells are vulnerable to GPX4 inhibition. Nature *551*, 247–250. https://doi.org/10.1038/nature24297.

18. Viswanathan, V.S., Ryan, M.J., Dhruv, H.D., Gill, S., Eichhoff, O.M., Seashore-Ludlow, B., Kaffenberger, S.D., Eaton, J.K., Shimada, K., Aguirre, A.J., et al. (2017). Dependency of a therapy-resistant state of cancer cells on a lipid peroxidase pathway. Nature *547*, 453–457. https://doi.org/10.1038/nature23007.

19. Stockwell, B.R. (2022). Ferroptosis turns 10: Emerging mechanisms, physiological functions, and therapeutic applications. Cell *185*, 2401–2421. https://doi.org/10.1016/j.cell.2022.06.003.

20. Sharma, S.V., Lee, D.Y., Li, B., Quinlan, M.P., Takahashi, F., Maheswaran, S., McDermott, U., Azizian, N., Zou, L., Fischbach, M.A., et al. (2010). A chromatin-mediated reversible drug-tolerant state in cancer cell subpopulations. Cell *141*, 69–80. https://doi.org/10.1016/j.cell.2010.02.027.

21. Jin, H., Wang, L., and Bernards, R. (2023). Rational combinations of targeted cancer therapies: background, advances and challenges. Nat. Rev. Drug Discov. *22*, 213–234. https://doi.org/10.1038/s41573-022-00615-z.

22. Ramirez, M., Rajaram, S., Steininger, R.J., Osipchuk, D., Roth, M.A., Morinishi, L.S., Evans, L., Ji, W., Hsu, C.H., Thurley, K., et al. (2016). Diverse drug-resistance mechanisms can emerge from drug-tolerant cancer persister cells. Nat. Commun. *7*, 10690. https://doi.org/10.1038/ncomms10690.

23. Saleh, T., and Gewirtz, D.A. (2022). Considering therapy-induced senescence as a mechanism of tumour dormancy contributing to disease recurrence. Br. J. Cancer *126*, 1363–1365. https://doi.org/10.1038/s41416-022-01787-6.

24. Wang, L., Lankhorst, L., and Bernards, R. (2022). Exploiting senescence for the treatment of cancer. Nat. Rev. Cancer *22*, 340–355. https://doi.org/10.1038/s41568-022-00450-9.

25. Jochems, F., Thijssen, B., De Conti, G., Jansen, R., Pogacar, Z., Groot, K., Wang, L., Schepers, A., Wang, C., Jin, H., et al. (2021). The Cancer SENESCopedia: A delineation of cancer cell senescence. Cell Rep. *36*, 109441. https://doi.org/10.1016/j.celrep.2021.109441.

26. Figarol, S., Delahaye, C., Gence, R., Asslan, R., Pagano, S., Tardy, C., Colinge, J., Villemin, J.-P., Maraver, A., Ferrer, I., et al. (2024). Farnesyltransferase inhibition overcomes the adaptive resistance to osimertinib in *EGFR*-mutant NSCLC. Nat Commun *15*, 5345. https://doi.org/10.1038/s41467-024-49360-4.

27. Moosmann, B., and Behl, C. (2004). Selenoprotein synthesis and side-effects of statins. Lancet *363*, 892–894. https://doi.org/10.1016/S0140-6736(04)15739-5.

28. Zheng, J., and Conrad, M. (2020). The Metabolic Underpinnings of Ferroptosis. Cell Metabol. *32*, 920–937. https://doi.org/10.1016/j.cmet.2020.10.011.

29. Xue, Y., Martelotto, L., Baslan, T., Vides, A., Solomon, M., Mai, T.T., Chaudhary, N., Riely, G.J., Li, B.T., Scott, K., et al. (2017). An approach to suppress the evolution of resistance in BRAF(V600E)-mutant cancer. Nat. Med. *23*, 929–937. https://doi.org/10.1038/nm.4369.

30. Eisenhauer, E.A., Therasse, P., Bogaerts, J., Schwartz, L.H., Sargent, D., Ford, R., Dancey, J., Arbuck, S., Gwyther, S., Mooney, M., et al. (2009). New response evaluation criteria in solid tumours: revised RECIST guideline (version 1.1). Eur. J. Cancer *45*, 228–247. https://doi.org/10.1016/j.ejca.2008.10.026.

31. Lim, J.K.M., Delaidelli, A., Minaker, S.W., Zhang, H.F., Colovic, M., Yang, H., Negri, G.L., von Karstedt, S., Lockwood, W.W., Schaffer, P., et al. (2019). Cystine/glutamate antiporter xCT (SLC7A11) facilitates oncogenic RAS transformation by preserving intracellular redox balance. Proc. Natl. Acad. Sci. USA *116*, 9433–9442. https://doi.org/10.1073/pnas.1821323116.

32. Johnson, D.B., Menzies, A.M., Zimmer, L., Eroglu, Z., Ye, F., Zhao, S., Rizos, H., Sucker, A., Scolyer, R.A., Gutzmer, R., et al. (2015). Acquired BRAF inhibitor resistance: A multicenter meta-analysis of the spectrum and frequencies, clinical behaviour, and phenotypic associations of resistance mechanisms. Eur. J. Cancer *51*, 2792–2799. https://doi.org/10.1016/j.ejca.2015.08.022.

33. Mikubo, M., Inoue, Y., Liu, G., and Tsao, M.S. (2021). Mechanism of Drug Tolerant Persister Cancer Cells: The Landscape and Clinical Implication for Therapy. J. Thorac. Oncol. *16*, 1798–1809. https://doi.org/10.1016/j.jtho.2021.07.017.

34. Raha, D., Wilson, T.R., Peng, J., Peterson, D., Yue, P., Evangelista, M., Wilson, C., Merchant, M., and Settleman, J. (2014). The cancer stem cell marker aldehyde dehydrogenase is required to maintain a drug-tolerant tumor cell subpopulation. Cancer Res. *74*, 3579–3590. https://doi.org/10.1158/0008-5472.CAN-13-3456.

35. Dhimolea, E., de Matos Simoes, R., Kansara, D., Al'Khafaji, A., Bouyssou, J., Weng, X., Sharma, S., Raja, J., Awate, P., Shirasaki, R., et al. (2021). An Embryonic Diapause-like Adaptation with Suppressed Myc Activity Enables Tumor Treatment Persistence. Cancer Cell *39*, 240–256.e11. https://doi.org/10.1016/j.ccell.2020.12.002.

36. Oren, Y., Tsabar, M., Cuoco, M.S., Amir-Zilberstein, L., Cabanos, H.F., Hutter, J.C., Hu, B., Thakore, P.I., Tabaka, M., Fulco, C.P., et al. (2021).

Cycling cancer persister cells arise from lineages with distinct programs. Nature *596*, 576–582. https://doi.org/10.1038/s41586-021-03796-6.

37. Sahu, N., Stephan, J.P., Cruz, D.D., Merchant, M., Haley, B., Bourgon, R., Classon, M., and Settleman, J. (2016). Functional screening implicates miR-371-3p and peroxiredoxin 6 in reversible tolerance to cancer drugs. Nat. Commun. *7*, 12351. https://doi.org/10.1038/ncomms12351.
38. Zhang, Z., Qin, S., Chen, Y., Zhou, L., Yang, M., Tang, Y., Zuo, J., Zhang, J., Mizokami, A., Nice, E.C., et al. (2022). Inhibition of NPC1L1 disrupts adaptive responses of drug-tolerant persister cells to chemotherapy. EMBO Mol. Med. *14*, e14903. https://doi.org/10.15252/emmm.202114903.
39. Shen, S., Faouzi, S., Souquere, S., Roy, S., Routier, E., Libenciuc, C., Andre, F., Pierron, G., Scoazec, J.Y., and Robert, C. (2020). Melanoma Persister Cells Are Tolerant to BRAF/MEK Inhibitors via ACOX1-Mediated Fatty Acid Oxidation. Cell Rep. *33*, 108421. https://doi.org/10.1016/j.celrep.2020.108421.
40. Hong, X., Roh, W., Sullivan, R.J., Wong, K.H.K., Wittner, B.S., Guo, H., Dubash, T.D., Sade-Feldman, M., Wesley, B., Horwitz, E., et al. (2021). The Lipogenic Regulator SREBP2 Induces Transferrin in Circulating Melanoma Cells and Suppresses Ferroptosis. Cancer Discov. *11*, 678–695. https://doi.org/10.1158/2159-8290.CD-19-1500.
41. Aloia, A., Mullhaupt, D., Chabbert, C.D., Eberhart, T., Fluckiger-Mangual, S., Vukolic, A., Eichhoff, O., Irmisch, A., Alexander, L.T., Scibona, E., et al. (2019). A Fatty Acid Oxidation-dependent Metabolic Shift Regulates the Adaptation of BRAF-mutated Melanoma to MAPK Inhibitors. Clin. Cancer Res. *25*, 6852–6867. https://doi.org/10.1158/1078-0432.CCR-19-0253.
42. Zhang, G., Frederick, D.T., Wu, L., Wei, Z., Krepler, C., Srinivasan, S., Chae, Y.C., Xu, X., Choi, H., Dimwamwa, E., et al. (2016). Targeting mitochondrial biogenesis to overcome drug resistance to MAPK inhibitors. J. Clin. Invest. *126*, 1834–1856. https://doi.org/10.1172/JCI82661.
43. Chang, M.T., Tsai, L.C., Nakagawa-Goto, K., Lee, K.H., and Shyur, L.F. (2022). Phyto-sesquiterpene lactones DET and DETD-35 induce ferroptosis in vemurafenib sensitive and resistant melanoma via GPX4 inhibition and metabolic reprogramming. Pharmacol. Res. *178*, 106148. https://doi.org/10.1016/j.phrs.2022.106148.
44. Dudnik, E., Peled, N., Nechushtan, H., Wollner, M., Onn, A., Agbarya, A., Moskovitz, M., Keren, S., Popovits-Hadari, N., Urban, D., et al. (2018). BRAF Mutant Lung Cancer: Programmed Death Ligand 1 Expression, Tumor Mutational Burden, Microsatellite Instability Status, and Response to Immune Check-Point Inhibitors. J. Thorac. Oncol. *13*, 1128–1137. https://doi.org/10.1016/j.jtho.2018.04.024.
45. Alvarez, S.W., Sviderskiy, V.O., Terzi, E.M., Papagiannakopoulos, T., Moreira, A.L., Adams, S., Sabatini, D.M., Birsoy, K., and Possemato, R. (2017). NFS1 undergoes positive selection in lung tumours and protects cells from ferroptosis. Nature *551*, 639–643. https://doi.org/10.1038/nature24637.
46. Terzi, E.M., Sviderskiy, V.O., Alvarez, S.W., Whiten, G.C., and Possemato, R. (2021). Iron-sulfur cluster deficiency can be sensed by IRP2 and regulates iron homeostasis and sensitivity to ferroptosis independent of IRP1 and FBXL5. Sci. Adv. *7*, eabg4302. https://doi.org/10.1126/sciadv.abg4302.
47. Hu, K., Li, K., Lv, J., Feng, J., Chen, J., Wu, H., Cheng, F., Jiang, W., Wang, J., Pei, H., et al. (2020). Suppression of the SLC7A11/glutathione axis causes synthetic lethality in KRAS-mutant lung adenocarcinoma. J. Clin. Invest. *130*, 1752–1766. https://doi.org/10.1172/JCI124049.
48. Muller, F., Lim, J.K.M., Bebber, C.M., Seidel, E., Tishina, S., Dahlhaus, A., Stroh, J., Beck, J., Yapici, F.I., Nakayama, K., et al. (2022). Elevated FSP1 protects KRAS-mutated cells from ferroptosis during tumor initiation. Cell Death Differ. *30*, 442–456. https://doi.org/10.1038/s41418-022-01096-8.
49. Chen, M., Mainardi, S., Lieftink, C., Velds, A., de Rink, I., Yang, C., Kuiken, H.J., Morris, B., Edwards, F., Jochems, F., et al. (2024). Targeting of vulnerabilities of drug-tolerant persisters identified through functional genetics delays tumor relapse. Cell Rep. Med. *5*, 101471. https://doi.org/10.1016/j.xcrm.2024.101471.
50. Madorsky Rowdo, F.P., Baron, A., Gallagher, S.J., Hersey, P., Emran, A.A., Von Euw, E.M., Barrio, M.M., and Mordoh, J. (2020). Epigenetic inhibitors eliminate senescent melanoma BRAFV600E cells that survive long-term BRAF inhibition. Int. J. Oncol. *56*, 1429–1441. https://doi.org/10.3892/ijo.2020.5031.
51. Maertens, O., Kuzmickas, R., Manchester, H.E., Emerson, C.E., Gavin, A.G., Guild, C.J., Wong, T.C., De Raedt, T., Bowman-Colin, C., Hatchi, E., et al. (2019). MAPK Pathway Suppression Unmasks Latent DNA Repair Defects and Confers a Chemical Synthetic Vulnerability in BRAF-NRAS- and NF1-Mutant Melanomas. Cancer Discov. *9*, 526–545. https://doi.org/10.1158/2159-8290.CD-18-0879.
52. Smith, M.P., and Wellbrock, C. (2016). Molecular Pathways: Maintaining MAPK Inhibitor Sensitivity by Targeting Nonmutational Tolerance. Clin. Cancer Res. *22*, 5966–5970. https://doi.org/10.1158/1078-0432.CCR-16-0954.
53. Jonas, O., Oudin, M.J., Kosciuk, T., Whitman, M., Gertler, F.B., Cima, M.J., Flaherty, K.T., and Langer, R. (2016). Parallel In Vivo Assessment of Drug Phenotypes at Various Time Points during Systemic BRAF Inhibition Reveals Tumor Adaptation and Altered Treatment Vulnerabilities. Clin. Cancer Res. *22*, 6031–6038. https://doi.org/10.1158/1078-0432.CCR-15-2722.
54. Huijberts, S., Wang, L., de Oliveira, R.L., Rosing, H., Nuijen, B., Beijnen, J., Bernards, R., Schellens, J., and Wilgenhof, S. (2020). Vorinostat in patients with resistant *BRAF*^{V600E} mutated advanced melanoma: a proof of concept study. Future Oncol. *16*, 619–629. https://doi.org/10.2217/fon-2020-0023.
55. Embaby, A., Huijberts, S., Wang, L., Leite de Oliveira, R., Rosing, H., Nuijen, B., Sanders, J., Hofland, I., van Steenis, C., Kluin, R.J.C., et al. (2024). A proof-of-concept study of sequential treatment with the HDAC inhibitor vorinostat following BRAF and MEK inhibitors in BRAFV600mutated melanoma. Clin. Cancer Res. https://doi.org/10.1158/1078-0432.CCR-23-3171.
56. Joung, J., Konermann, S., Gootenberg, J.S., Abudayyeh, O.O., Platt, R.J., Brigham, M.D., Sanjana, N.E., and Zhang, F. (2017). Genome-scale CRISPR-Cas9 knockout and transcriptional activation screening. Nat. Protoc. *12*, 828–863. https://doi.org/10.1038/nprot.2017.016.
57. Bolger, A.M., Lohse, M., and Usadel, B. (2014). Trimmomatic: a flexible trimmer for Illumina sequence data. Bioinformatics *30*, 2114–2120. https://doi.org/10.1093/bioinformatics/btu170.
58. Li, B., and Dewey, C.N. (2011). RSEM: accurate transcript quantification from RNA-Seq data with or without a reference genome. BMC Bioinf. *12*, 323. https://doi.org/10.1186/1471-2105-12-323.
59. Korotkevich, G., Sukhov, V., Budin, N., Shpak, B., Artyomov, M.N., and Sergushichev, A. (2021). Fast gene set enrichment analysis. Preprint at bioRxiv, 060012. https://doi.org/10.1101/060012.
60. Liberzon, A., Birger, C., Thorvaldsdottir, H., Ghandi, M., Mesirov, J.P., and Tamayo, P. (2015). The Molecular Signatures Database (MSigDB) hallmark gene set collection. Cell Syst. *1*, 417–425. https://doi.org/10.1016/j.cels.2015.12.004.
61. Hanzelmann, S., Castelo, R., and Guinney, J. (2013). GSVA: gene set variation analysis for microarray and RNA-seq data. BMC Bioinf. *14*, 7. https://doi.org/10.1186/1471-2105-14-7.
62. Nokin, M.J., Darbo, E., Travert, C., Drogat, B., Lacouture, A., San Jose, S., Cabrera, N., Turcq, B., Prouzet-Mauleon, V., Falcone, M., et al. (2020). Inhibition of DDR1 enhances in vivo chemosensitivity in KRAS-mutant lung adenocarcinoma. JCI insight *5*, e137869. https://doi.org/10.1172/jci.insight.137869.

STAR★METHODS

KEY RESOURCES TABLE

REAGENT or RESOURCE	SOURCE	IDENTIFIER
Antibodies		
Rabbit monoclonal anti-PD-L1 (clone 28-8)	Abcam	Cat#ab205921; RRID: AB_2687878
Rabbit monoclonal anti-PD-L2 (clone D7U8C)	Cell signaling Technology	Cat#82723; RRID:AB_2799999
Rabbit monoclonal anti-CD47 (clone D307P)	Cell signaling Technology	Cat#63000; RRID:AB_2799637
Rabbit monoclonal anti-VISTA (clone D5L5T)	Cell signaling Technology	Cat#54979; RRID:AB_2799474
Rabbit monoclonal anti-CD200 (clone E519V)	Cell signaling Technology	Cat#23451; RRID:AB_3102027
Rabbit polyclonal anti-B7H3 (CD276)	Thermo Fisher Scientific	Cat#PA5-114525; RRID:AB_2890419
Rabbit monoclonal anti-keratin 7 (clone SP52)	Roche Diagnostics	Cat# 05986818001; RRID: AB_3102028
Rabbit polyclonal anti-GPX4	Abcam	Cat# ab231174; RRID:AB_3073732
Rabbit polyclonal anti-4 Hydroxynonenal	Abcam	Cat# ab46545; RRID:AB_722490
Rabbit monoclonal anti-xCT/SLC7A11 (clone D2M7A)	Cell signaling Technology	Cat#12691; RRID:AB_2687474
Rabbit monoclonal anti-4F2hc/SLC3A2 (clone D3F9D)	Cell signaling Technology	Cat#47213; RRID:AB_2799323
Rabbit polyclonal anti-GPX4	Cell signaling Technology	Cat#52455; RRID:AB_2924984
Rabbit monoclonal anti-BRAF (clone 55C6)	Cell signaling Technology	Cat#9433; RRID:AB_2259354
Rabbit monoclonal anti-Phospho-MEK1/2 Ser217/221 (clone 41G9)	Cell signaling Technology	Cat#9154; RRID:AB_2138017
Rabbit monoclonal anti-MEK1/2 (clone D1A5)	Cell signaling Technology	Cat#8727; RRID:AB_10829473
Rabbit polyclonal anti-Phospho-p44/42 MAPK (Erk1/2) Thr202/Tyr204	Cell signaling Technology	Cat#9101; RRID:AB_331646
Mouse monoclonal anti-p44/42 MAPK (Erk1/2) (clone L34F12)	Cell signaling Technology	Cat#4696; RRID:AB_390780
Rabbit monoclonal anti-Phospho-Akt Ser473 (clone D9E)	Cell signaling Technology	Cat#4060; RRID:AB_2315049
Rabbit monoclonal anti-Phospho-Akt Thr308 (clone D25E6)	Cell signaling Technology	Cat#13038; RRID:AB_2629447
Rabbit polyclonal anti-Akt	Cell signaling Technology	Cat#9272; RRID:AB_329827
Rabbit monoclonal anti-Phospho-EGF Receptor Tyr1068 (clone D7A5)	Cell signaling Technology	Cat#3777; RRID:AB_2096270
Rabbit monoclonal anti-EGF Receptor (clone D38B1)	Cell signaling Technology	Cat#4267; RRID:AB_2246311
Rabbit monoclonal anti-Phospho-Histone H3 Ser10 (clone D2C8)	Cell signaling Technology	Cat#3377; RRID:AB_1549592
Rabbit monoclonal anti-Histone H3 (clone D1H2)	Cell signaling Technology	Cat#4499; RRID:AB_10544537
Rabbit monoclonal anti-CD71/TFRC (clone D7G9X)	Cell signaling Technology	Cat#13113; RRID:AB_2715594
Rabbit monoclonal anti-FTH1 (clone D1D4)	Cell signaling Technology	Cat#4393; RRID:AB_11217441
Rabbit monoclonal anti-HSP90 (clone C45G5)	Cell signaling Technology	Cat#4877; RRID:AB_2233307
Goat polyclonal anti-NRAS	Abcam	Cat#ab77392; RRID:AB_1524048
Rabbit polyclonal anti-acetyl-Histone H3	Merck	Cat#06–599; RRID:AB_2115283
Rabbit polyclonal anit-Actin	Merck	Cat#A2066; RRID:AB_476693
Mouse monoclonal anti-α-Tubulin (clone B-5-1-2)	Merck	Cat#T6074; RRID:AB_477582
Anti-goat IgG, HRP-linked antibody	Thermo Fisher Scientific	Cat#A15999; RRID:AB_2534673
Anti-rabbit IgG, HRP-linked Antibody	Cell signaling Technology	Cat#7074; RRID:AB_2099233
Anti-mouse IgG, HRP-linked Antibody	Cell signaling Technology	Cat#7076; RRID:AB_330924
Anti-rabbit IgG EnVision+ HRP	Agilent	Cat# K400311-2
Biological samples		
Pleural effusions at baseline and after treatment from a *BRAF*^{V600E} NSCLC patient	DanaFarber Cancer Institute (DF/HCC 02–180)	N/A

(*Continued on next page*)

Continued

REAGENT or RESOURCE	SOURCE	IDENTIFIER
Chemicals, peptides, and recombinant proteins		
Dabrafenib mesylate	TargetMol	Cat#T8474
Trametinib	TargetMol	Cat#T125
RSL3	TargetMol	Cat#T3646
Erastin	TargetMol	Cat#T1765
FIN56	TargetMol	Cat#T4066
Trolox	TargetMol	Cat#T1710
Ferrostatin-1	TargetMol	Cat#T6500
Liproxstatin-1	TargetMol	Cat#T2376
Deferoxamine mesylate	TargetMol	Cat#T8474
Vorinostat	TargetMol	Cat#T1583
Panobinostat	TargetMol	Cat#T2383
Lovastatin	TargetMol	Cat#T1207
Simvastatin	TargetMol	Cat#T0687
Atorvastatin	TargetMol	Cat#T20765
Fluvastatin sodium	TargetMol	Cat#T1487
N-acetyl-L-cysteine (NAC)	Merck	Cat#A7250
Sodium selenite	Merck	Cat#214485
Critical commercial assays		
GSH-Glo™ Glutathione Assay	Promega	Cat#V6911
CellROX™ Green Flow Cytometry Assay kit	Thermo Fisher Scientific	Cat#C10492
FerroOrange Assay Kit	Dojindo Laboratories	Cat#F374
BODIPY™ 665/676 (Lipid Peroxidation Sensor)	Thermo Fisher Scientific	Cat#B3932
FITC Annexin V Apoptosis Detection Kit I	BD Biosciences	Cat#556547
Deposited data		
RNA-seq data	This paper	GEO:GSE271247
Experimental models: Cell lines		
HCC364	Dana-Farber Cancer Institute, authenticated by Eurofins Genomics using the Applied Biosystems AmpFLSTR Identifier Plus	RRID:CVCL_5134
DFCI471	Dana-Farber Cancer Institute[14]	N/A
1D and 1E PDX-derived cell lines	Prof. P. Lito[29]	N/A
Experimental models: Organisms/strains		
NSG mice	Charles River	Strain code 614
Oligonucleotides		
qRT-PCR sequences	This paper	See Table S1
sgRNA sequences	This paper	See Table S2
Recombinant DNA		
pLVX-HA-NRAS^{Q61K}	This paper	N/A
pLKO.1-TRC shRNA control	MISSION (Merck)	N/A
pLKO.1-TRCN0000033256 (shNRAS#1)	MISSION (Merck)	N/A
pLKO.1-TRCN0000033257 (shNRAS#2)	MISSION (Merck)	N/A
HP138-puro	Dr. I. Cheeseman	Addgene Plasmid #134246
TLCV2	Dr. A. Karpf	Addgene Plasmid #87360
lenti-sgRNA blast	Dr. B. Stringer	Addgene Plasmid #104993
Human sgRNA library Brunello in lentiGuide-Puro	Dr. D. Root & J. Doench	Addgene Plasmid #73178
pJS10-Cas9 blast	This paper	N/A
pLenti6-CMV-luciferase	This paper	N/A

(*Continued on next page*)

Continued

REAGENT or RESOURCE	SOURCE	IDENTIFIER
Software and algorithms		
GraphPad Prism8	GraphPad	https://www.graphpad.com
QuPath 0.4.3	QuPath	https://qupath.github.io/
CRISPRAnalyzeR		https://github.com/boutroslab/CRISPRAnalyzeR
MAGeCK		https://sourceforge.net/projects/mageck/
R version 4.1	R Core Team 2017	https://www.r-project.org

RESOURCE AVAILABILITY

Lead contact

Further information and requests for resources and reagents should be directed to and will be fulfilled by the lead contact, David Santamaría (d.santamaria@usal.es).

Materials availability

Further requests for cell lines generated in this study should be directed to and will be fulfilled by the lead contact, David Santamaría (d.santamaria@usal.es), with the Materials Transfer Agreement.

Data and code availability

Original/source data of RNA-sequencing (accession number: GSE271247) have been deposited at https://www.ncbi.nlm.nih.gov/geo/and are publicly available as of the date of publication. This study did not report new original code. Any additional information required to reanalyse the data reported in this paper is available from the lead contact upon request.

EXPERIMENTAL MODEL AND STUDY PARTICIPANT DETAILS

Cell lines and cell culture

Human *BRAF*^{V600E}-mutant lung adenocarcinoma cell line HCC364 was obtained from the Dana Farber Cancer Institute. DFCI471 cells were derived from a fresh biopsy of a *BRAF*^{V600E}-mutated LUAD patient who progressed following D/T treatment.[14] These cells were maintained *in vitro* in presence of a high concentration of dabrafenib (1μM). *BRAF*^{V600E}-mutant PDX-derived cell lines (clone 1D and 1E) generated from a patient at disease progression after treatment with a RAF inhibitor[29] at Prof. Lito's laboratory (Memorial Sloan Kettering Cancer Center, New York, NY, USA). All cell lines were regularly checked for mycoplasma contamination using MycoAlert Mycoplasma Detection Kit (Lonza). Cells were either cultured in standard DMEM (HCC364 and derivatives, 1D and 1E cells) or in RPMI-1640 (DFCI471 cells) medium both containing 10% fetal bovine serum (FBS, ThermoFisher Scientific), 2 mM L-glutamine (ThermoFisher Scientific) and 1% penicillin-streptomycin (ThermoFisher Scientific).

Generation of cell line derivatives: HCC364-DTPs, DTEPs and EGFRa were generated by treating HCC364 cells with 250 nM dabrafenib and 5 nM trametinib (D/T 250/5 nM) for 3, 40 and 70 weeks, respectively. 1D-DTPs and 1E-DTPs were obtained by treating parental 1D and 1E PDX-derived cells with D/T 250/5 nM for 3 weeks 1D-DTEPs were generated by maintaining the D/T 250/5 nM treatment for 40 weeks 1E-DTEPs were generated by maintaining the D/T 250/5 nM treatment for 30 weeks. From this point onwards a cell line derivative containing a *BRAF* gene amplification (CNV 15.4) was generated and was referred to as 1E-R. In all cases, the drugs were refreshed every 3 days. In order to determine if long-term D/T treated cells acquired a genetic alterations as resistance mechanism, these cells were cultured in absence of D/T (drug holiday) for 3 weeks and, then, treated again with the drugs. The proliferation of these rechallenged cells was followed during 1 week and compared to long term cells constantly cultured with D/T (250/5 nM). HCC364^{NRAS} cells were generated by lentiviral transduction of pLVX-HA-NRAS^{Q61K} in HCC364 DTPs, allowing resistance to D/T by exogenous expression of *NRAS*^{Q61K} mutant.

Animals and *in vivo* studies

All animal experimental procedures were performed according to the Federation of European Laboratory Animal Sciences Associations (FELASA). The procedures were reviewed and approved either by the Ethic Committee of the University of Bordeaux (France) under the number APAFIS #15445 or by the Institutional Animal Care and Ethics Committee of the University of Liège (Belgium) under the number 22–2422. Female 6-week-old NSG mice were purchased from Charles River (strain code 614). All animals were housed either in the Animal Facility A2 of the University of Bordeaux (institutional agreement number: A33063916) or in the GIGA-accredited animal facility of the University of Liège (institutional agreement number: LA1610002).

For subcutaneous xenografts, $2.5x10^6$ DFCI471 cells were resuspended in 100 μL RPMI supplemented with 20% (v/v) matrigel (BD Biosciences) and were inoculated subcutaneously in one flank of 8-week-old female NSG mice. Tumor volume was measured with a caliper using the formula W x W x L/2, where W and L denote width and length, respectively. When tumor volume reached 150 mm^3, mice were randomized in 3 groups and treated with vehicle, vorinostat (100 mg/kg/day) or panobinostat (10 mg/kg/day) by intraperitoneal injection 5 days per week (n = 10 per condition). Drugs were dissolved in 5% DMSO, 30% PEG-300 and 5% Tween-80 solution. After 2 weeks, mice were sacrificed and tumors were collected. One piece was embedded in paraffin for IHC and the rest was frozen in liquid nitrogen for total protein extraction.

For lung orthotopic implantation, PDX-1D cells were first stably transduced with pLenti6-CMV-luciferase and selected with 10 μg/mL blasticidin. One million 1D cells were resuspended in 50 μL DMEM with 20% (v/v) matrigel and were implanted by transcutaneous intralung injection in 8-week-old female NSG mice. Tumor growth was monitored using bioluminescence imaging once a week. When tumors started to grow (18 days post-implantation), mice were treated with a combination of dabrafenib (30 mg/kg/day) and trametinib (0.2 mg/kg/day) by oral gavage 5 days per week (n = 15 D/T and 3 vehicle mice). When D/T treated tumors reached a volume 20% higher to that estimated at the beginning of the drug treatment (disease progression), mice were randomized in 2 groups and treated with RSL3 (10 mg/kg/day) by intraperitoneal injection 5 days per week (n = 6–7 per condition). All drugs were dissolved in 5% DMSO, 30% PEG-300 and 2% Tween-80 solution. After 2 weeks, mice were sacrificed and lungs were collected for further analysis.

Patient sample

Pre and post D/T treatment samples were obtained from a 74 years old male patient with a $BRAF^{V600E}$ mutated NSCLC, who gave his written informed consent to the correlative protocol DF/HCC 02–180. Two samples were included in this study: a baseline pleural effusion and a recurrent pleural effusion. Tumor DNA only sequencing using the DFCI OncoPanel platform, and immunohistochemistry (described in methods details) were performed on both these samples. The protocol DF/HCC 02–180 was approved by the Dana-Farber Cancer Institute IRB.

METHOD DETAILS

shRNA-mediated NRAS knock-down

The following vectors from the MISSION library were used: MISSION pLKO.1- TRC shRNA control, TRCN0000033256 and TRCN0000033257 targeting human NRAS. Cells were infected with lentiviral particles and selected with Puromycin 1 μg/ml in order to obtain stable populations.

GPX4 and SLC7A11 inducible CRISPR-Cas9 Knock-out

Parental cell lines (HCC364-DTPs and HCC364-EGFRa) were co-transfected with transposase and hp138-puro (a gift from Iain Cheeseman –Addgene plasmid # 134246–) and selected with puromycin to generate doxycycline-inducible Cas9 derivatives. HCC364-NRAS were infected with lentiviral particles generated using TLCV2 (a gift from Adam Karpf –Addgene plasmid # 87360–) and FACS-sorted using the GFP reporter. In all cases expression of Cas9 was confirmed by western blotting. Cells were subsequently infected with lentiviral particles generated using plenti-sgRNA blast (a gift from Brett Stringer –Addgene plasmid # 104993–) and selected with blasticidin. The specific sgRNA sequences are listed in Tables S2.

Genome-wide sgRNA library construction

In this study, the human Brunello CRISPR knockout sgRNA library (Addgene #73178), a gift from David Root and John Doench (Broad Institute, Boston, USA), was used to identify genes responsible for D/T resistance in HCC364 cells. This pooled library contains 76,441 unique sgRNA sequences targeting 19114 protein-coding genes (4 sgRNAs/gene) and 1000 control non-targeting sgRNAs. Amplification of pooled sgRNA library, lentivirus production and titer determination were performed as previously described.[56]

CRISPR/Cas9 screening for determinants of dabrafenib/trametinib sensitivity

The workflow of this screen is illustrated in Figure 1A. First, we generated a stable Cas9-expressing HCC364 cells (HCC364-Cas9) by lentiviral transduction of pJS10-Cas9 plasmid (MOI = 1) and selection with blasticidin. Both the expression and the activity of Cas9 were validated by western blot and FACS analysis using control sgRNAs, respectively. Then we transduced HCC364-Cas9 cells with the Brunello library at a MOI of 0.3 aiming for coverage of, on average, 1,000 cells per sgRNA. The positively transduced cells were selected with 1 μg/mL of puromycin for 7 days to generate a mutant cell pool. $8x10^7$ cells, representing the baseline of sgRNAs representation, were collected for further analysis. This latter was then treated with vehicle (DMSO) or 250 nM dabrafenib and 5 nM trametinib for 3 weeks (medium was replaced every 3–4 days). After the treatment, at least $8x10^7$ cells were harvested for genomic DNA extraction using Quick-DNA Midiprep plus kit (Zymo Research D4075). Illumina sequencing libraries were generated using PCR amplification with primers specific to the genome integrated lentiviral vector backbone sequence, as previously described.[56] These libraries were sequenced with a MiSeq instrument (Illumina). The number of reads was adjusted to cover each sgRNA with approximately 1000 reads.

CRISPR/cas9 screening data analysis

Fastq files were processed (screen quality, read cleaning and mapping) and analyzed (hit calling) using CRISPRAnalyzeR.[10] Hit calling was performed using MaGECK and a Z-Ratio was calculated between the pre-treated and treated cells.

RNA-sequencing and data analysis

Transcriptome sequencing (RNA-seq) was performed in parental, DTP and DTEP-HCC364 cells. Fastq files from different lanes were merged and sequencing quality was analyzed using FastQC version 0.11.9 (https://www.bioinformatics.babraham.ac.uk/projects/fastqc/). Reads were trimmed using trimmomatic version 0.39[57] using parameters LEADING:30 TRAILING:30 MINLEN:36. Read mapping and gene quantification were performed using RSEM version 1.3.2[58] with STAR aligner and default parameters.

Gene Set Enrichment Analysis (GSEA) was performed with fgsea R package version 1.20.0[59] on estimated Transcript Per Million (TPM) log fold-changes with KEGG, Reactome, Wikipathway and Hallmark gene sets from MSig database version 7[60] as well as drug tolerance gene signature.[26] The score computation to evaluate the activity of E2F targets (Hallmarks) and cell cycle checkpoints (Reactome) pathways was performed following single sample GSEA method by using GSVA R package version 1.42.0[61] on log2 transformed TPM with parameters method = "ssgsea", min.sz = 10, ssgsea.norm = T. Senescence score was computed from RNA-seq raw counts with the online tool SENCAN - cancer senescence classifier (https://rhpc.nki.nl/sites/senescence/classifier.php) reached on the August the 10th 2022.

GSH measurement

Cells were seeded in 96-well white plates and cultured overnight at 37°C in a 5% CO_2 incubator. Glutathione (GSH) intracellular concentration was assessed using GSH-Glo Glutathione Assay (V6911, Promega) following the manufacturer's instructions.

ROS measurement

The cells were treated in presence of drugs for 72 h. ROS production by cancer cell lines was measured using CellROX Green Flow Cytometry assay kit (C10492, ThermoFisher Scientific) according to the manufacturer's protocol.

Intracellular iron measurement

Intracellular ferrous ion (Fe^{2+}) levels were determined by flow cytometry using FerroOrange probe (F374-10, Dojindo). Briefly, 24 h after seeding, cells were washed with HBSS three times. After trypsinization, the cell suspension in complete medium was transferred to a FACS tube and was centrifuged at 1,500 rpm for 3 min. The cell pellet was washed once with HBSS and then, was resuspended in serum-free DMEM medium with 0.2 μM FerroOrange. A negative control was performed by adding 1 μM of deferoxamine. The cells were incubated for 15–30 min in a 37°C incubator equilibrated with 5% CO_2. The samples were analyzed using a LSRFortessa flow cytometer (BD Biosciences).

Peroxidized lipids content measurement

Peroxidized lipids content was measured using the lipid peroxidation probe BODIPY 665/676 (B3932, ThermoFisher Scientific). The cells were treated in the presence of drugs (Erastin, RSL3 and Trolox) for 72 h. After trypsinization, the cell pellet was resuspended in 4 μM BODIPY staining solution in PBS and incubated in the dark for 20 min at 37°C. The cells were washed with PBS 3 times and analyzed using a FACSCanto II flow cytometer (BD Biosciences).

Cell growth assay

For IC50 determination assays, 12-points serial dilutions of the different drugs/compounds (Dabrafenib, Trametinib, Erastin, RSL3, FIN56, Trolox, Ferrostatin-1, Liproxstatin-1, Deferoxamine, Vorinostat, Panobinostat, Lovastatin, Simvastatin, Atorvastatin, Fluvastatin, N-acetyl-L-cysteine and sodium selenite) were added to 96-well plates containing cells (HCC364, 3,000 cells per well; DFCI471, 1D and 1E, 5,000 cells per well). After 72 h incubation, cell viability was determined using MTT reagent and absorbance was read at 595 nm on a spectrophotometer plate reader. For proliferation curve assays, cell viability was measured at day 1, 3, 5 and 7 after treatment with D/T (refreshed every 3 days).

Clonogenic assay

Cells were seeded into 6-well plates (10,000 cells per well) and cultured with the indicated drugs (Dabrafenib, Trametinib, Vorinostat, Panobinostat and N-acetyl-L-cysteine) for 10–15 days. At the end of the assay, cells were fixed with 4% of formaldehyde and stained with 2% of crystal violet. After photo scanning, crystal violet was released by cell lysis using 5% SDS solution and quantified by absorbance measurement using a spectrophotometer plate reader.

Apoptosis assay

HCC364 cells were treated with Dabrafenib/Trametinib (D/T 250/5 nM) for 24, 48 and 72 h. Cells were collected and apoptosis was measured with the FITC Annexin V Apoptosis Detection Kit I (BD Biosciences) using a FACSCanto II flow cytometer (BD Biosciences).

Immunohistochemistry

Following the deparaffinization step, tissue sections were autoclaved for 11 min at 126°C in 10 mM citrate buffer (pH6), Target Retrieval Solution (S1699, Dako) or in Tris/EDTA buffer (pH9). Endogenous peroxidases were blocked by incubation in 3% H_2O_2 solution for 20 min and slides were incubated with animal free blocking solution (15019L, Cell Signaling) for 20 min at room temperature (RT). The following antibodies were used for the primary reaction [1 h at room temperature in diluent solution (S2022, Dako)]: anti-PD-L1 (1/300, clone 28-8, Abcam), anti-PD-L2 (1/200, clone D7U8C, Cell Signaling), anti-CD47 (1/400, clone D307P, Cell Signaling), anti-VISTA (1/400, clone D5L5T, Cell Signaling), anti-CD200 (1/200, clone E519V, Cell Signaling), anti-B7-H3 (1/1500, polyclonal, #PA5-114525, ThermoFisher Scientific), anti-keratin 7 (ready to use, clone SP52, Ventana Medical Systems), anti-GPX4 (1/500, ab231174, Abcam) and anti-4-hydroxynonenal (4-HNE, 1/400, ab46545, Abcam). After washes in PBS, the secondary reaction was performed using the rabbit Envision+/HRP (Agilent Technologies) according to the manufacturer's recommendations. Positive cells were visualized using SignalStain DAB Substrate Kit (Cell Signaling). Samples were counterstained with hematoxylin and mounted with EUKITT (Kindler GmbH). For anti-GPX4 and anti-4-HNE antibodies, the intensity of the staining (0, 1+, 2+, 3+) in tumor cells was assessed in three independent immunolabeled tissue sections and results are expressed as mean of these three scores per lung. Regarding the expression of immune checkpoints by tumor cells, the number of positive cells per mm^2 was precisely determined by computerized counts (QuPath 0.4.3 software for digital pathology image analysis).

Somatic variants analysis

DNA samples were screened for somatic variants by using the 'Solid Tumor Solution' (Sophia Genetics SA, Switzerland) according to the manufacturer's protocol. Sequencing was performed on a MiSeq platform using v3 chemistry (Illumina, USA). Data were analyzed using the Sophia DDM Platform with Sophia Genetics proprietary algorithms.

Cystine uptake

Cells were seeded in 96-well back plates and cultured overnight at 37°C in a 5% CO_2 incubator. Cystine uptake by cancer cells was measured using the Cystine uptake assay kit (UP05-12, Dojindo) according to the manufacturer's protocol.

Western blotting

Cells were extracted in RIPA buffer (150 mM NaCl, 0.5% Na+-deoxycholate, 1% Triton X-100, 0.1% SDS, 50 mM Tris-HCl pH 7.5 and protease/phosphatase inhibitors). Protein concentrations were determined using the DC Protein Assay kit (Bio-Rad). Twenty μg of proteins were separated by 7.5–12.5% SDS-PAGE and transferred to PVDF or nitrocellulose membranes. Membranes were saturated for 1h with blocking buffer [5% skim milk in tris-buffered saline with 0.1% Tween 20 (TBS-T)] for 1 h at room temperature (RT) and probed overnight in primary antibody at 4°C. The following primary antibodies raised against xCT/SLC7A11 (#12691), 4F2hc/CD98/SLC3A2 (#47213), GPX4 (#52455), BRAF (#9433), phospho-MEK1/2 S217/221 (#9154), MEK1/2 (#8727), phospho-ERK1/2 T202/Y204 (#9101), ERK1/2 (#4696), P-AKT S473 (#4060), P-AKT T308 (#13038), AKT (#9272), phospho-EGFR Y1068 (#3777), EGFR (#4267), phospho-Histone H3 S10 (#3377), histone H3 (#4499), TFRC (#13113), FTH1 (#4393) and HSP90 (#4877) were purchased from Cell Signaling Technology. Antibodies also included those raised against NRAS (ab77392, Abcam), acetyl-Histone H3 (06–599, Sigma-Aldrich), actin (A2066, Sigma-Aldrich) and alpha-tubulin (T6074, Sigma-Aldrich). After three washes, the membranes were exposed to appropriate secondary HRP-linked antibody (anti-rabbit IgG #7074 or anti-mouse IgG #7076 antibodies from Cell Signaling Technology or anti-goat IgG #A15999 from Thermo Fisher Scientific) at RT for 1 h. The immunoreactive bands were visualized using Clarity Western ECL Substrate (Bio-Rad).

RNA extraction, reverse transcription and quantitative PCR (RT-qPCR)

Total cellular RNA was extracted reverse-transcribed and then subjected to PCR amplification and quantification, as previously described.[62] Briefly, one microgram of total cellular RNA, extracted using the Quick-RNA MiniPrep Plus Kit (Zymo Research), was reverse-transcribed utilizing the OneScript cDNA Synthesis Kit (Abm). The resulting cDNA was then amplified by PCR with SsoAdvanced Universal SYBR Green Supermix (Bio-Rad). The PCR signals were captured using a CFX384 Touch Real-Time PCR System and analyzed with Bio-Rad's CFX Manager software. Primer sequences are listed in Table S1.

QUANTIFICATION AND STATISTICAL ANALYSIS

All experiments were performed as several independent biological replicates. All results were reported as means with standard deviation (SD) or Standard Error Mean (SEM) as indicated in figure legends. The number of biological replicates as well as the number of animals in treatment groups are indicated in the figure legends. Two group comparisons were performed using unpaired Student's t test with or without Welsch's correction according to homoscedasticity. When an experiment required comparisons between more than two groups, statistical analysis was performed using one-way or two-way ANOVA depending on the number of grouping factors. Dunnett's or Tukey's post-test was applied for simple or multiple comparisons, respectively. In the case of discrete variables (IHC scores), the comparison between groups was performed by Mann-Whitney's U test. In all cases, a bilateral $p < 0.05$ was considered as statistically significant with a 95% confidence interval. Statistical tests are indicated in figure legends and exact p values are indicated in the figures. All analyses were conducted with GraphPad Prism 8 (GraphPad Software, USA).

Cell Reports Medicine, Volume *5*

Supplemental information

In vivo vulnerabilities to GPX4 and HDAC inhibitors in drug-persistent versus drug-resistant $BRAF^{V600E}$ lung adenocarcinoma

Marie-Julie Nokin, Elodie Darbo, Elodie Richard, Sonia San José, Sergio de Hita, Valérie Prouzet-Mauleon, Béatrice Turcq, Laura Gerardelli, Rebekah Crake, Valérie Velasco, Benjamin Koopmansch, Frederic Lambert, Jenny Y. Xue, Ben Sang, Julie Horne, Eric Ziemons, Alberto Villanueva, Arnaud Blomme, Michael Herfs, Didier Cataldo, Olivier Calvayrac, Paolo Porporato, Ernest Nadal, Piro Lito, Pasi A. Jänne, Biagio Ricciuti, Mark M. Awad, Chiara Ambrogio, David Santamaría, and Bolero Consortium

Supplemental information

In vivo vulnerabilities to GPX4 and HDAC inhibitors in drug-persistent versus drug-resistant $BRAF^{V600E}$ lung adenocarcinoma

Marie-Julie Nokin, Elodie Darbo, Elodie Richard, Sonia San José, Sergio de Hita, Valérie Prouzet-Mauleon, Béatrice Turcq, Laura Gerardelli, Rebekah Crake, Valérie Velasco, Benjamin Koopmansch, Frederic Lambert, Jenny Y Xue, Ben Sang, Julie Horne, Eric Ziemons, Alberto Villanueva, Arnaud Blomme, Michael Herfs, Didier Cataldo, Olivier Calvayrac, Paolo Porporato, Ernest Nadal, Piro Lito, Pasi A. Janne, Biagio Ricciuti, Mark Awad, Chiara Ambrogio & David Santamaría

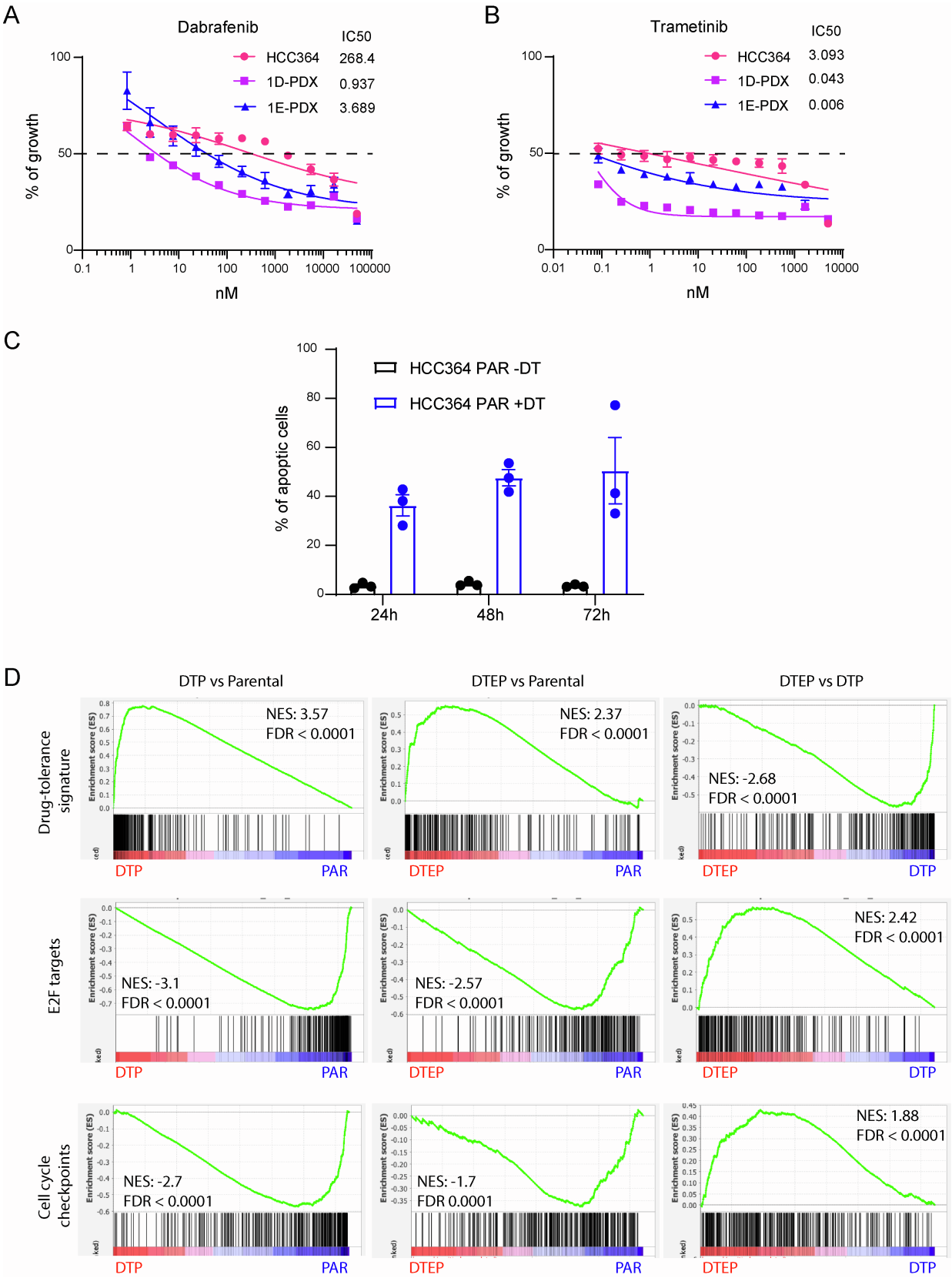

Figure S1: Characterization of HCC364 DTP and DTEP states following D/T treatment, related to Figures 1, 2 and 4. A, B. Cell viability assessment by MTT assay of HCC364, 1D- and 1E-PDX cells treated with serial dilutions of dabrafenib (A) and trametinib (B) for 72 hr. IC50 values are indicated for each condition. *n* = 3 biological replicates. **C.**

Apoptosis quantification by flow cytometry of HCC364 cells treated with 250/5 nM dabrafenib/trametinib for 24, 48 and 72 hr. *n* = 3 biological replicates. **D.** Enrichment scores of GSEA in DTP vs Parental, DTEP vs Parental and DTEP vs DTP using the drug tolerance signature and the E2F targets and cell cycle checkpoints gene sets. *n* = 1 biological replicate. All data are shown as the mean values ± SEM.

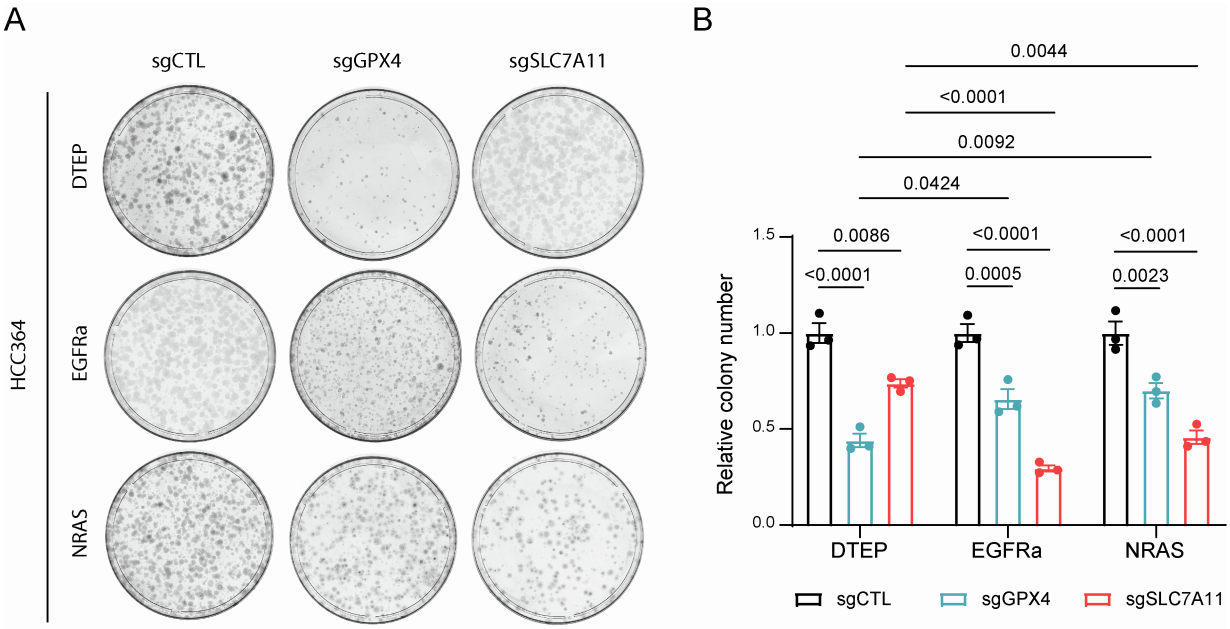

Figure S2: Clonogenic assay following Crispr/Cas9 knock-out of GPX4 and SLC7A11 in DTEP and D/T resistant HCC364 cells, related to Figures 3 and 5. Clonogenic assay of the indicated HCC364 cell line variants cultured with 250/5 nM dabrafenib/trametinib and 1µg/ml doxycycline to induce Crispr/Cas9 mediated knock-out of GPX4 or SLC7A11. An sgRNA targeting LacZ was used as control. Data are shown as the mean values ± SEM. *n* = 3 biological replicates.

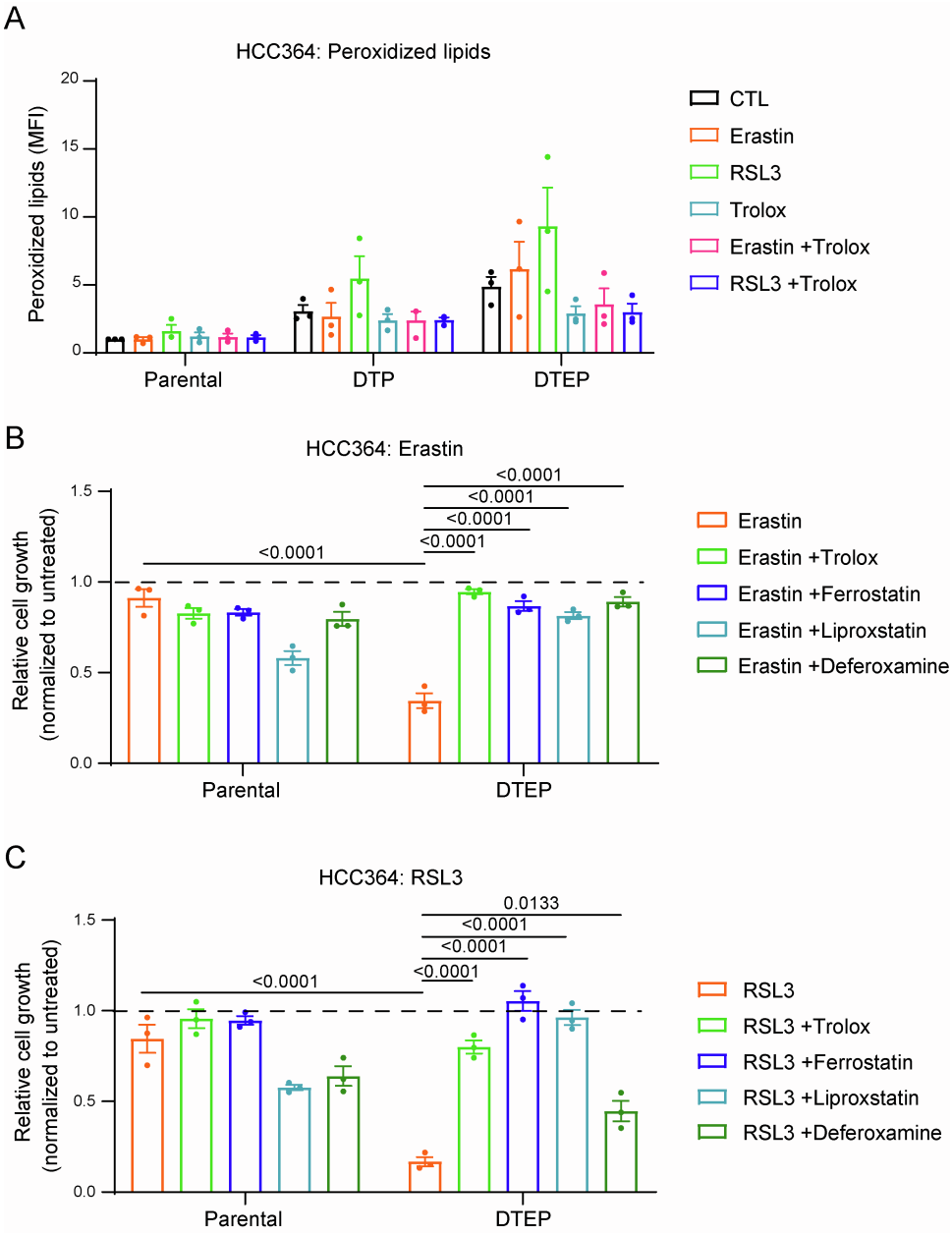

Figure S3: Rescue experiment of RSL3-treated HCC364 DTEPs upon co-incubation with ferroptosis inhibitors, related to Figure 3. A. Intracellular peroxidized lipids content in parental, DTP and DTEP HCC364 cells treated with 500 nM Erastin or 50 nM RSL3 in presence of 10 µM Trolox for 72 hr. Data are shown as the mean values ± SEM. *n* = 3 biological replicates. **B, C.** Cell viability assessment by MTT assay of parental and DTEP HCC364 cells treated with 500 nM Erastin (B) or 50 nM RSL3 (B) in presence of 10 µM Trolox, 200 nM Ferrostatin, 100 nM Liproxstatin, 1 µM Deferoxamine for 72 hr. Data are normalized to untreated cells and shown as the mean values ± SEM. Data were analysed using two-way ANOVA followed by Tukey's multiple comparisons post-test. *n* = 3 biological replicates.

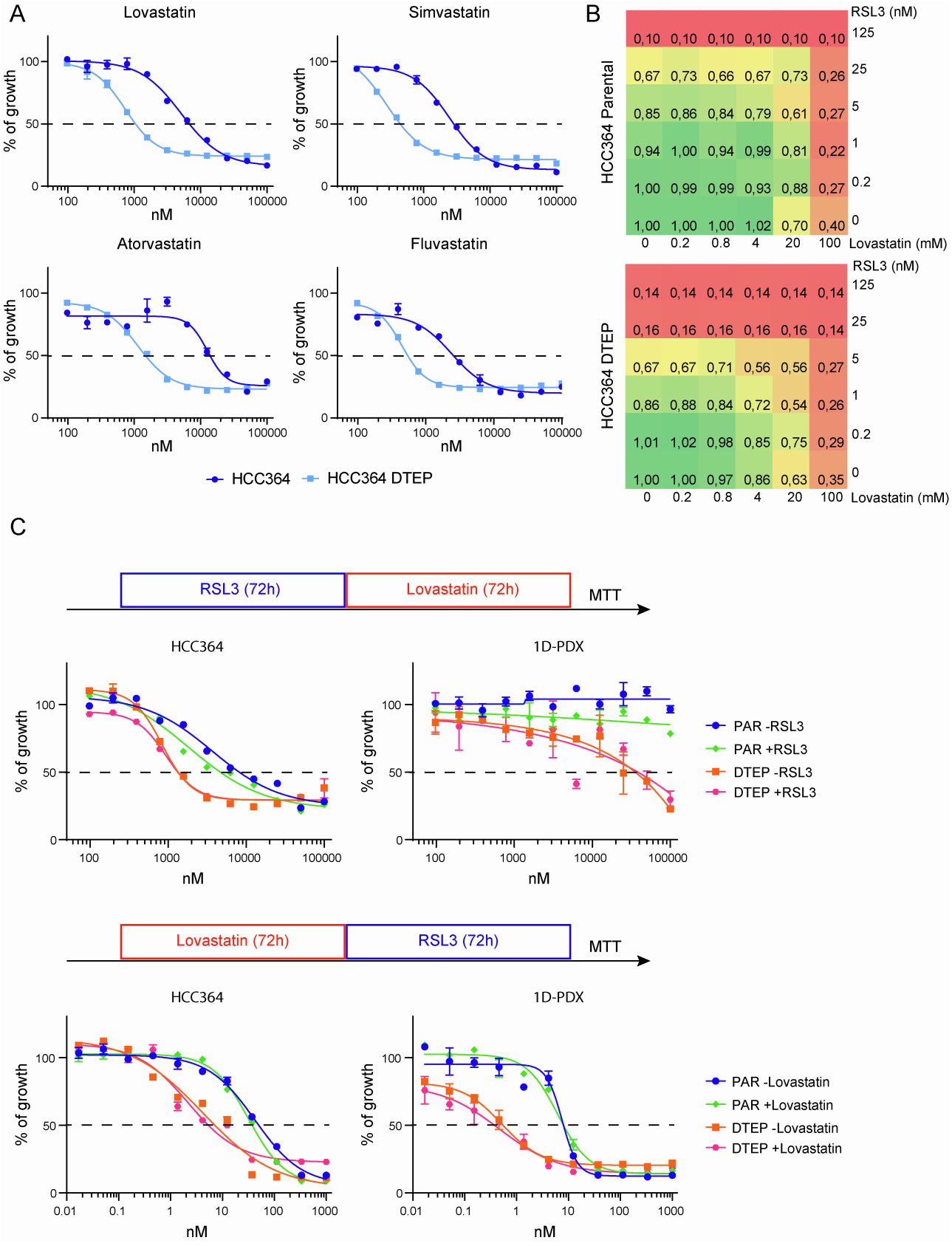

Figure S4: Treatment combinations of the GPX4 inhibitor RSL3 and statins in HCC364 and PDX-derived cell line 1D, related to Figure 3. A. Cell viability assessment by MTT assay of parental and DTEP HCC364 cells treated

with serial dilutions of the indicated drugs for 72 hr. *n* = 3 biological replicates. **B.** Sensitivity matrix comparing parental and DTEP HCC364 cells after 72 hr in presence of the indicated concentrations of RSL3 and Lovastatin. *n* = 3 biological replicates. **C.** Cell viability assessment by MTT assay of parental and DTEP HCC364 and 1D-PDX cells treated with serial dilutions of Lovastatin (upper panels) or RSL3 (lower panels) for 72 hr after a pretreatment (72 hr) with RSL3 1 nM or Lovastatin 1 μM, respectively. *n* = 3 biological replicates. All data are shown as the mean values ± SEM of one representative experiment.

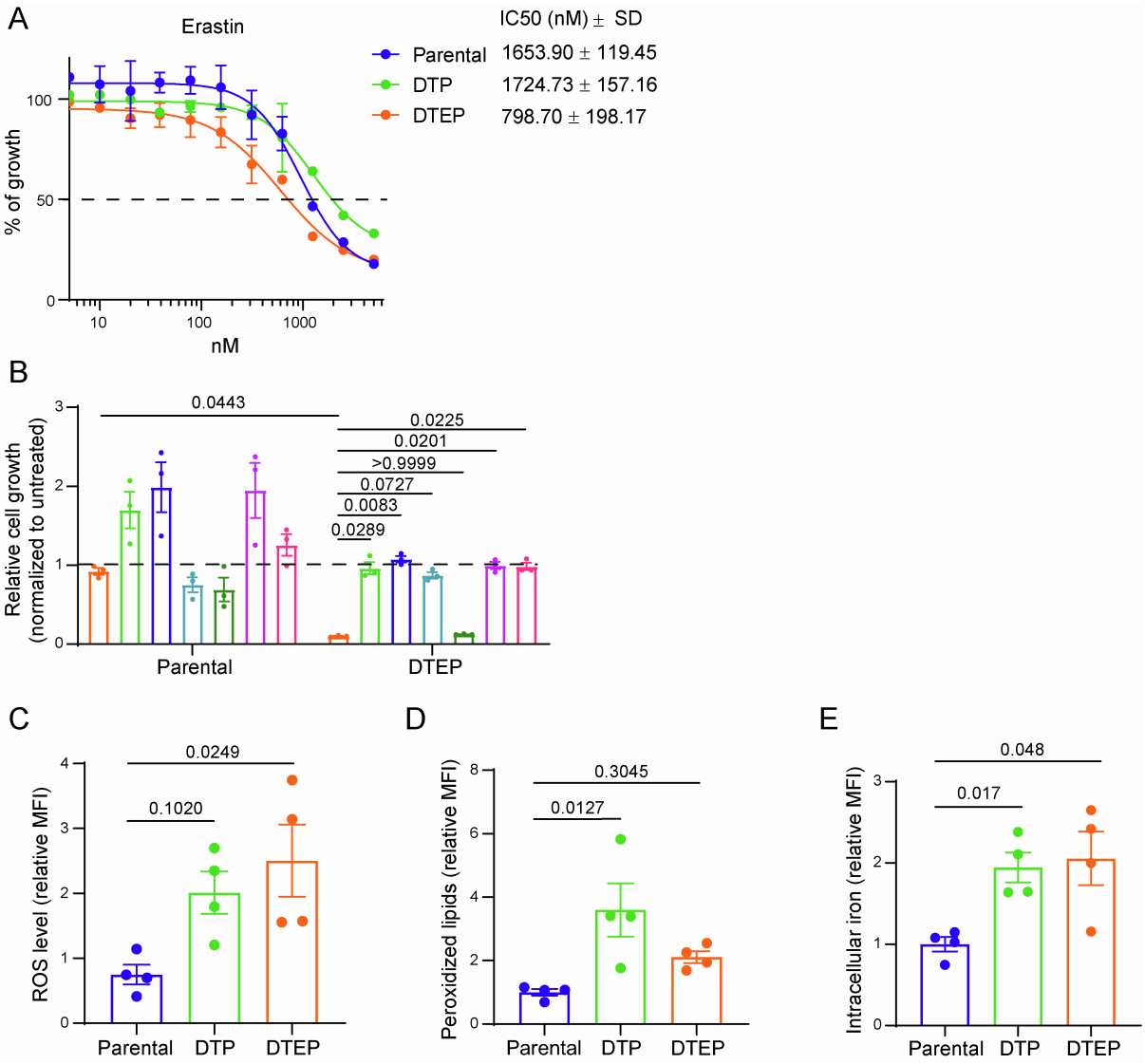

Figure S5: PDX-derived cell line 1D DTP & DTEPs are sensitive to ferroptosis triggers, related to Figure 4. A. Cell viability assessment by MTT assay of parental (PAR), DTP and DTEP 1D cells treated with serial dilutions of Erastin for 72 hr. Data are shown as the mean values ± SEM. IC50 values ± SD are indicated for each condition. *n* = 3 biological replicates. **B.** Cell viability assessment by MTT assay of parental and DTEP 1D cells treated with 500 nM Erastin in presence of 10 µM Trolox, 200 nM Ferrostatin, 100 nM Liproxstatin, 1 µM Deferoxamine, 200 nM selenium (Se) or 2.5 mM N-acetyl-cysteine (NAC) for 72 hr. Data are normalized to untreated cells and shown as the mean values ± SEM. Data were analysed using two-way ANOVA followed by Tukey's multiple comparisons post-test. *n* = 3 biological replicates. **C-E.** Intracellular ROS level (C), peroxidized lipids content (D) and iron level (E) in parental, DTP and DTEP 1D cells. Data were analysed using one-way ANOVA followed by Dunnett's multiple comparisons post-test and are shown as the mean values ± SEM. *n* = 4 biological replicates.

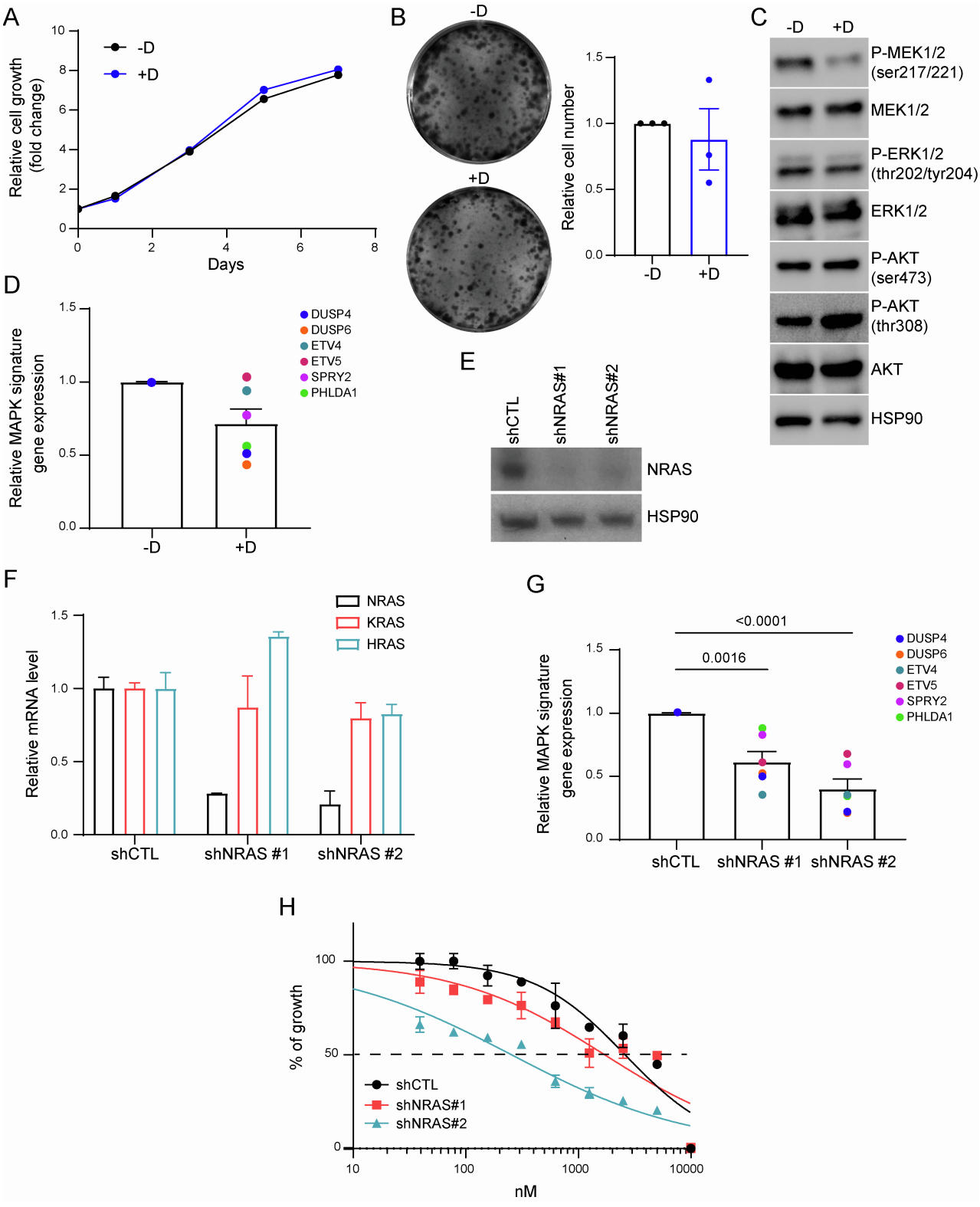

Figure S6: An acquired *NRAS*^{Q61K} mutation drives D/T resistance in DFCI471 cells, related to Figure 5. A. Growth curves of DFCI471 cells in presence of 1 µM dabrafenib. Data are shown as the mean values ± SEM of one representative experiment. *n* = 3 biological replicates. **B.** Clonogenic assay of DFCI471 cells cultured with 1 µM dabrafenib. Data are shown as the mean values ± SEM. *n* = 3 biological replicates. **C.** Immunoblot of phospho-MEK1/2, -ERK1/2 and -AKT in DFCI471 cells cultured in presence of 1µM dabrafenib (D) for 48 hr. HSP90 was used

as a loading control. *n* = 2 biological replicates. **D.** Quantitative RT-PCR analysis of relative MAPK pathway target genes (DUSP4, DUSP6, ETV4, ETV5, SPRY2, PHLDA1) mRNA levels in DFCI471 cells cultured in presence of 1μM dabrafenib (+D) for 48 hr. Data are shown as the mean values ± SEM. *n* = 3 biological replicates. **E.** Immunoblot of NRAS in DFCI471 upon NRAS shRNAs (shNRAS #1 and #2) mediated knock-down. *n* = 2 biological replicates. **F and G.** Quantitative RT-PCR analysis of relative NRAS, KRAS and HRAS mRNA levels (F) and of relative MAPK pathway target genes (DUSP4, DUSP6, ETV4, ETV5, SPRY2, PHLDA1) mRNA levels (G) in NRAS knock-down DFCI471 cells. Data are shown as the mean values ± SEM. *n* = 3 biological replicates. **H.** Cell viability assessment by MTT assay of DFCI471 cells upon NRAS shRNAs (shNRAS #1 and #2) mediated knock-down treated with serial dilutions of Dabrafenib for 72 hr. Data are shown as the mean values ± SEM. *n* = 3 biological replicates.

A

IC50 (nM, 72h)	Dabrafenib	Trametinib
HCC364	274	1.5
HCC364^{NRAS}	> 1000	> 50

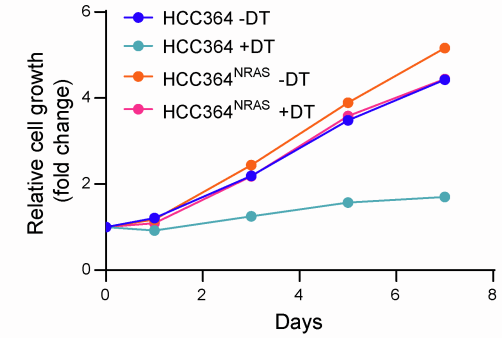

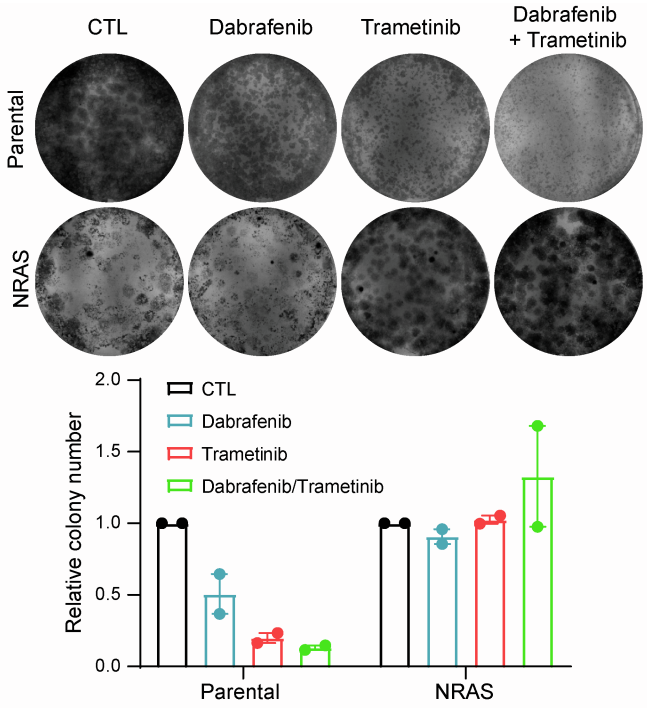

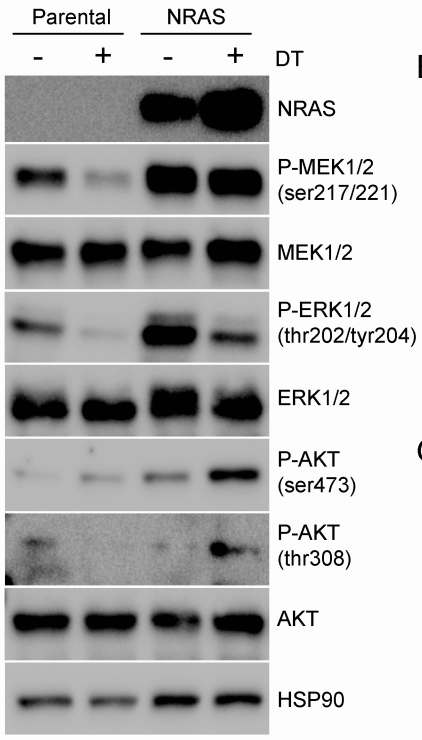

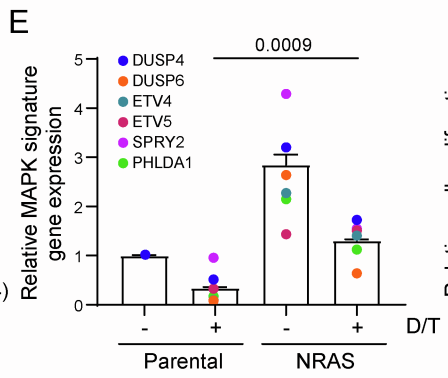

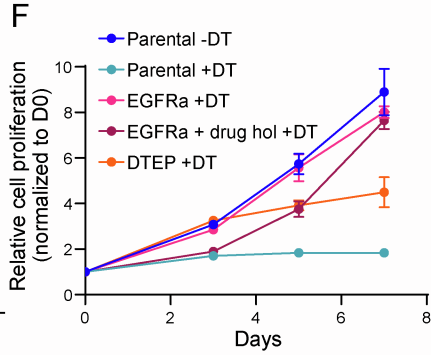

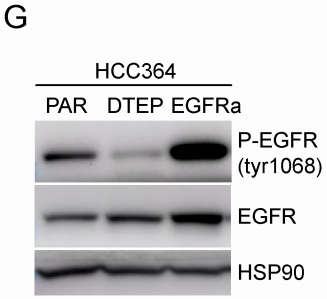

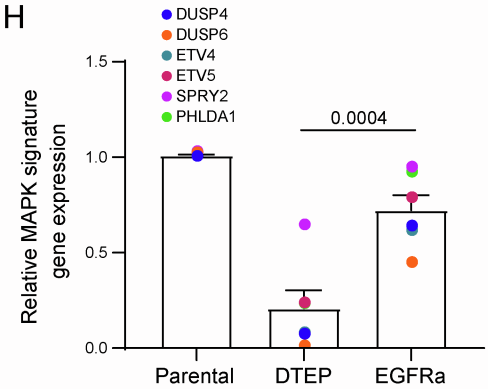

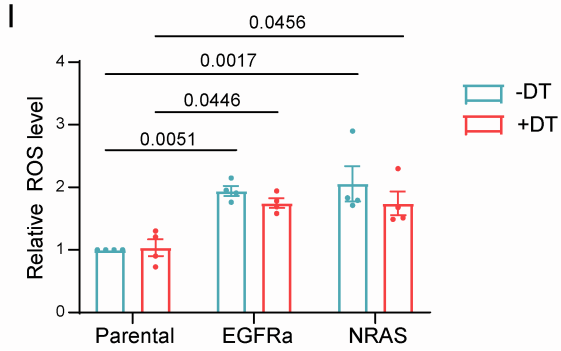

Figure S7: Acquired mutations resulting in MAPK reactivation drive D/T resistance in HCC364 cells, related to Figure 5. A. Cell viability assessment by MTT assay of HCC364 and HCC364^{NRAS} cells treated with serial dilutions of dabrafenib or trametinib for 72 hr. IC50 values are indicated for each condition. *n* = 3 biological replicates. **B.** Clonogenic assay of HCC364 and HCC364^{NRAS} cells treated with 250 nM dabrafenib, 5 nM trametinib or 250/5 nM dabrafenib/trametinib. Data are shown as the mean values ± SEM. *n* = 2 biological replicates. **C.** Growth curves of HCC364 and HCC364^{NRAS} cells in presence of 250/5 nM dabrafenib/trametinib (+DT). Data are shown as the mean values ± SEM of one representative experiment. *n* = 3 biological replicates. **D.** Immunoblot of NRAS, phospho-MEK1/2, -ERK1/2 and -AKT in HCC364 and HCC364^{NRAS} cells cultured in presence of 250/5 nM D/T (DT) for 48 hr. HSP90 was used as a loading control. *n* = 2 biological replicates. **E.** Quantitative RT-PCR analysis of relative MAPK pathway target genes (DUSP4, DUSP6, ETV4, ETV5, SPRY2, PHLDA1) mRNA levels in HCC364 and HCC364^{NRAS} cells cultured in presence of 250/5 nM D/T for 48 hr. Data were analysed using one-way ANOVA followed by Tukey's multiple comparisons post-test and are shown as the mean values ± SEM. *n* = 3 biological replicates. **F.** HCC364^{EGFRa} were derived spontaneously from HCC364-DTEPs after continuous D/T (250/5 nM) treatment for 70 weeks. Growth curves of parental, DTEP and EGFRa HCC364 cells in presence of 250/5 nM D/T. EGFRa cells undergone a drug holiday for 3 weeks and were rechallenged with D/T to confirm the genetic adaptation of these cells to the treatment (EGFRa + drug hol +DT). Data are shown as the mean values ± SEM of one representative experiment. *n* = 3 biological replicates. **G.** Immunoblot of phospho-EGFR in parental, DTEP and EGFRa HCC364 cells. HSP90 was used as a loading control. *n* = 3 biological replicates. **H.** Quantitative RT-PCR analysis of relative MAPK pathway target genes (DUSP4, DUSP6, ETV4, ETV5, SPRY2, PHLDA1) mRNA levels in parental, DTEP and EGFRa HCC364 cells. Data are shown as the mean values ± SEM. *n* = 3 biological replicates. **I.** Intracellular ROS level in HCC364 and HCC364^{NRAS} cells cultured in presence of 250/5 nM D/T (+DT) for 72 hr. Data were analysed using two-way ANOVA followed by Tukey's multiple comparisons post-test and are shown as the mean values ± SEM. *n* = 4 biological replicates.

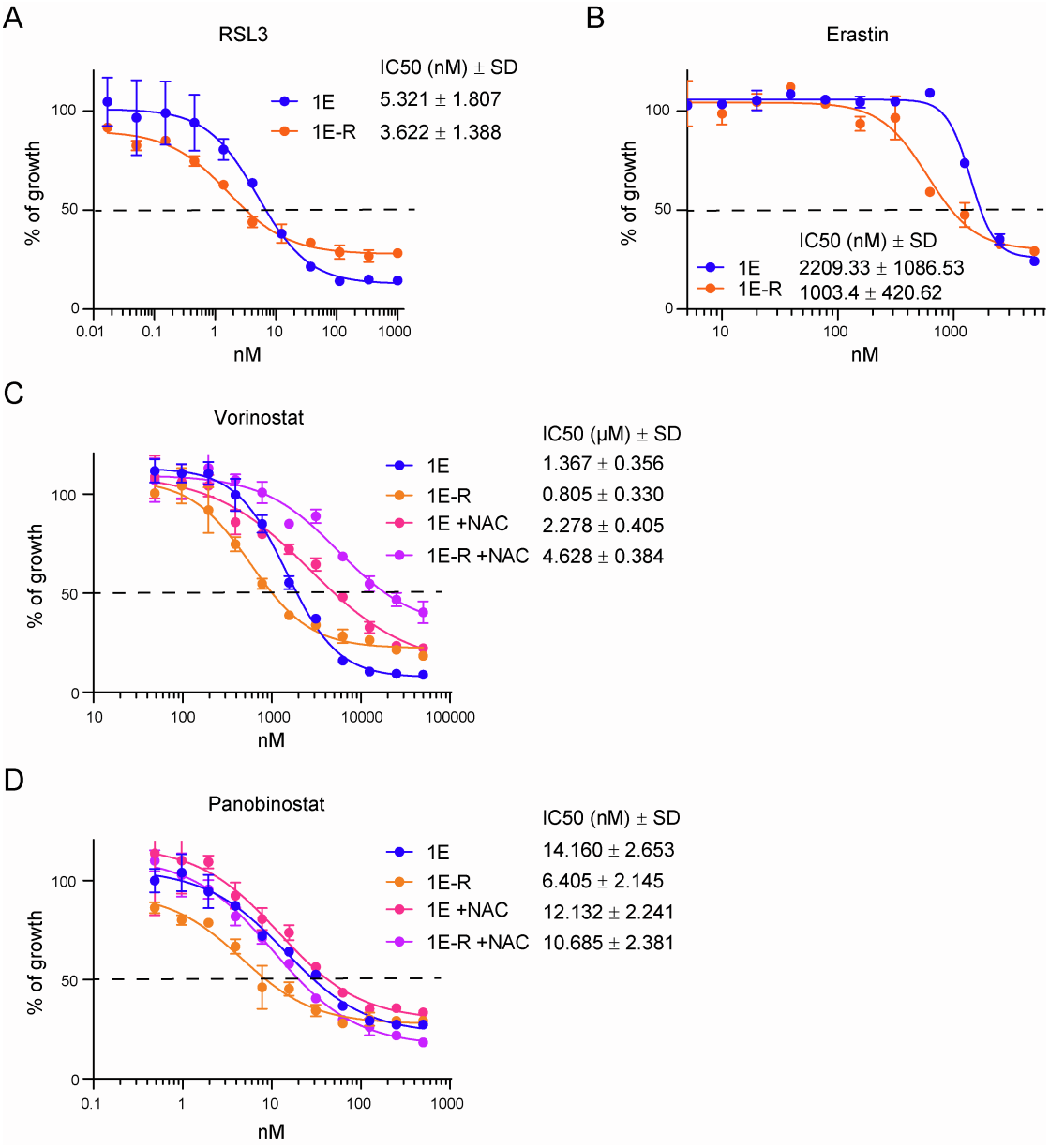

Figure S8: D/T resistant PDX-derived cell line 1E are insensitive to ferroptosis triggers and sensitive to HDAC inhibition, related to Figure 6. A, B. Cell viability assessment by MTT assay of 1E and 1E-R cells treated with serial dilutions of RSL3 (A) and Erastin (B) for 72 hr. *n* = 3 biological replicates. **C, D.** Cell viability assessment by MTT assay of 1E and 1E-R cells treated with serial dilutions of vorinostat (C) and panobinostat (D) in presence of 2.5 mM NAC for 72 hr. *n* = 3 biological replicates. All data are shown as the mean values ± SEM. IC50 values ± SD are indicated for each condition.

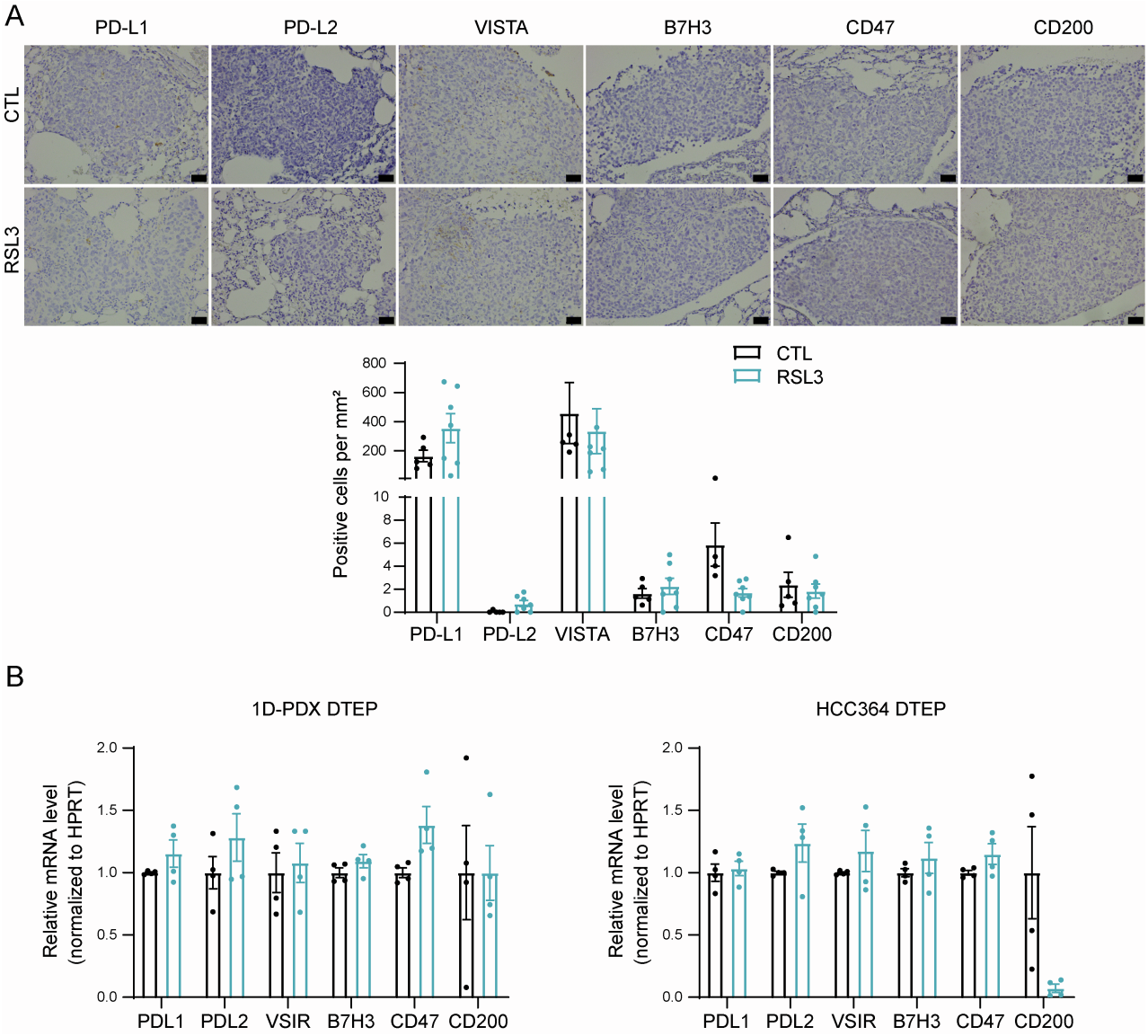

Figure S9: *In vitro* & *in vivo* evaluation of various immune-checkpoint related proteins at the DTEP stage upon GPX4 inhibition, related to Figure 4. A. Representative PD-L1, PD-L2, VISTA, B7H3, CD47 and CD200 immunostaining in lung sections of mice treated with RSL3 (upper panel). Scale bars represent 50 µm. Quantification of immune checkpoint proteins staining scores (per mice) in 1D tumours from mice treated with vehicle or with RSL3 (lower panel). *n* = 5 or 7 mice per group. **B.** Quantitative RT-PCR analysis of relative immune checkpoint genes (*PDL1, PDL2, VSIR, B7H3, CD47 and CD200*) mRNA levels in DTEP 1D-PDX and HCC364 cells cultured in presence of RSL3 1 nM for 48 hr. Data are shown as the mean values ± SEM. *n* = 4 biological replicates.

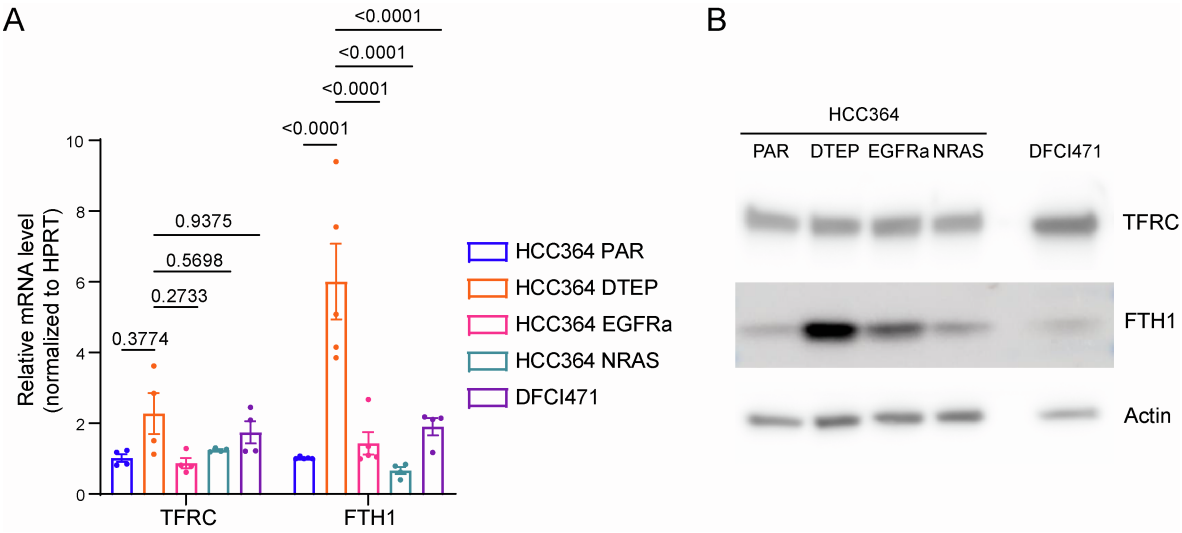

Figure S10: Evaluation of TFRC & FTH1 expression in DTEP and acquired resistance settings, related to Figures 3 and 5. A. Quantitative RT-PCR analysis of relative TFRC and FTH1 mRNA levels in parental and DTEP HCC364, HCC364^{EGFRa}, HCC364^{NRAS} and DFCI471 cells. Data were analysed using one-way ANOVA followed by Tukey's multiple comparisons post-test and are shown as the mean values ± SEM. *n* = 4 biological replicates. **B.** Immunoblot of TFRC and FTH1 in parental and DTEP HCC364, HCC364^{EGFRa}, HCC364^{NRAS} and DFCI471 cells. Actin was used as a loading control. *n* = 2 biological replicates.

Table S1: Primer sequences used for RT-PCR. Related to STAR Methods.

Human gene	Forward primer	Reverse primer
SLC7A11	5′- AGCACATAGCCAATGGTGAC-3′	5′-GCTGGCTGGTTTTACCTCAA-3′
DUSP4	5’- GGCGGCTATGAGAGGTTTTCC-3’	5’-TGGTCGTGTAGTGGGGTCC -3’
DUSP6	5’- GAAATGGCGATCAGCAAGACG-3’	5’- CGACGACTCGTATAGCTCCTG-3’
ETV4	5’- CAGTGCCTTTACTCCAGTGCC-3’	5’- CTCAGGAAATTCCGTTGCTCT-3’
ETV5	5’- CAGTCAACTTCAAGAGGCTTGG-3’	5’- TGCTCATGGCTACAAGACGAC-3’
SPRY2	5’-CCTACTGTCGTCCCAAGACCT-3’	5’- GGGGCTCGTGCAGAAGAAT-3’
PHLDA1	5’- GAAGATGGCCCATTCAAAAGCG-3	5’- GAGGAGGCTAACACGCAGG-3’
TFRC	5’-GGCTACTTGGGCTATTGTAAAGG-3’	5’-CAGTTTCTCCGACAACTTTCTCT-3’
FTH1	5’-TGAAGCTGCAGAACCAACGAGG-3’	5’-GCACACTCCATTGCATTCAGCC-3’
NRAS	5’- TGAGAGACCAATACATGAGGACA-3’	5’- CCCTGTAGAGGTTAATATCCGCA-3’
KRAS	5’- GGACTGGGGAGGGCTTTCT-3’	5’- GCCTGTTTTGTGTCTACTGTTCT-3’
HRAS	5’- GACGTGCCTGTTGGACATC-3’	5’- CTTCACCCGTTTGATCTGCTC-3’
PDL1	5’-TGGCATTTGCTGAACGCATTT-3’	5’-TGCAGCCAGGTCTAATTGTTTT-3’
PDL2	5’-ATTGCAGCTTCACCAGATAGC-3’	5’-AAAGTTGCATTCCAGGGTCAC-3’
VSIR (VISTA)	5’-ACGCCGTATTCCCTGTATGTC-3’	5’-TTGTAGAAGGTCACATCGTGC-3’
B7H3	5’-TGTCTCATTGCACTGCTGGT-3’	5’-TGTCTTGGAGCCTTCTCCCT-3’
CD47	5’-AGAAGGTGAAACGATCATCGAGC-3’	5’-CTCATCCATACCACCGGATCT-3’
CD200	5’-ACGTCTGTTACCAGCATCCTC-3’	5’-CTTAAAGTCGGTCACAGTCCC-3’

Table S2: sgRNA sequences for CRISPR/Cas9 editing. Related to STAR Methods

Human gene	Forward primer	Reverse primer
GPX4	5’-CACCGTTTCCGCCAAGGACATCGAC-3’	5’-AAACGTCGATGTCCTTGGCGGAAAC-3’
SLC7A11	5’-CACCGGCAACATAGAATAACCTGAT-3’	5’-AAACATCAGGTTATTCTATGTTGCC-3’
LACZ Ctrl	5’-CACCGAGACGATCCGCTGGCCGTTA-3’	5’-AAACTAACGGCCAGCGGATCGTCTC-3’